The impact of the stellar distribution on the feedback of super star clusters

by

Sergio Martínez González

Thesis submitted in partial fulfillment of the requirements
for the degree of

MASTER OF SCIENCE IN ASTROPHYSICS

at the

Instituto Nacional de Astrofísica, Óptica y Electrónica

November 2011

Tonantzintla, Puebla

Advised by:

PhD. Sergiy Silich
Tenured Researcher INAOE
PhD. Guillermo Tenorio-Tagle
Tenured Researcher INAOE

Abstract

The thermalization of the kinetic energy provided by massive stars via stellar winds and supernova explosions inside young and coeval super star clusters (SSCs) causes the ejection of powerful gaseous outflows, the stellar cluster winds. These outflows affect significantly the interstellar medium of the host galaxy and can be detected in the optical, infrared and X-rays bands.

The original stationary solution for an adiabatic spherically symmetric cluster wind was proposed by Chevalier & Clegg (1985) and subsequently developed with numerical calculations by Cantó et al. (2000), Raga et al. (2001) and Rockefeller et al. (2005). The importance of radiative cooling in star cluster driven winds have been recognized by Silich et al. (2003). The radiative wind model has been discussed then in a series of papers (Silich et al., 2004, 2007; Tenorio-Tagle et al., 2007; Wünsch et al., 2008; Wünsch et al., 2011).

However, until now several significant simplifications have been made for the solution of the hydrodynamic equations. One of such simplifications is that the stars are homogeneously distributed within a star cluster volume with radius R_{sc} whereas observations demonstrate that stellar profiles are best fit with King models (Mengel et al., 2002).

Several attempts have been made in order to improve the model. Rodríguez-González et al. (2007) presented a model for winds driven by star clusters with a power-law stellar density distribution. However, the wind central density is infinite in this model in contrast to observations.

Ji et al. (2006) considered an exponential stellar density distribution in a one-dimensional numeric approach. However, none of these two models have taken into account the impact of radiative cooling on the star cluster driven wind hydrodynamics.

The major aim of this thesis is to develop a semi-analytic method which allows to solve the set of 1D hydrodynamic equations with account of the radiative gas cooling and obtain the distribution of the hydrodynamic variables (expansion velocity, wind temperature, particle number density, thermal pressure and ram pressure) for winds driven by star clusters with a more realistic stellar density distribution.

For a homogeneous stellar density distribution, the singular point, *i.e.* the radius at which the wind becomes supersonic, must be located at the star cluster surface (Chevalier & Clegg, 1985). However, for an exponential stellar density distribution, there is no star cluster surface and therefore the position of the singular point must be calculated.

In this thesis, a procedure that allows to calculate the position of the singular point in a self-consistent manner is proposed. The main result of this calculation is that in the quasi-adiabatic regime, the singular point is always located at four times the star cluster core radius from the star cluster center. Additionally, the ram pressure is equal to the thermal pressure at three times the star cluster core radius. On the other hand, in the catastrophic cooling regime, the wind temperature drops rapidly close to the singular point which is no longer located at four times the star cluster core radius and moves towards the star cluster center.

Resumen

La termalización de la energía cinética provista por estrellas masivas vía vientos estelares y explosiones de supernova dentro de súper cúmulos estelares (SSCs) jóvenes y coetáneos provoca la eyección de poderosos flujos gaseosos, los vientos de los cúmulos estelares. Estos flujos afectan significativamente el medio interestelar de la galaxia anfitriona y pueden ser detectados en las bandas energéticas óptica, infrarroja y de rayos-X.

La solución estacionaria original para el modelo adiabático de viento esféricamente simétrico fue propuesta por Chevalier & Clegg (1985) y posteriormente desarrollada con los cálculos numéricos de Cantó et al. (2000), Raga et al. (2001) y Rockefeller et al. (2005). La importancia del enfriamiento radiativo para los vientos producidos por cúmulos estelares fue reconocida por Silich et al. (2003). El modelo radiativo del viento de cúmulos estelares ha sido discutido desde entonces en una serie de artículos (Silich et al., 2004, 2007; Tenorio-Tagle et al., 2007; Wünsch et al., 2008; Wünsch et al., 2011).

Sin embargo, hasta ahora varias simplificaciones significativas se han usado para resolver las ecuaciones de hidrodinámica. Una de estas simplificaciones es que las estrellas se encuentran distribuidas homogéneamente dentro de un volumen del cúmulo estelar de radio R_{sc} a pesar de que las observaciones demuestran que los perfiles de densidad de estrellas en cúmulos estelares reales es mejor reproducida por los modelos de King (Mengel et al., 2002).

Se han hecho varios intentos para mejorar el modelo en lo que a esto respecta. Rodríguez-González et al. (2007) presentaron un modelo de vientos producidos por cúmulos estelares con una distribución de densidad estelar que sigue una ley de potencia. No obstante que en estos modelos la densidad central es infinita en contraste

con las observaciones.

Ji et al. (2006) abordaron el problema considerando una distribución de densidad estelar exponencial con un enfoque numérico unidimensional. Empero, ninguno de estos modelos ha incluído el enfriamiento radiativo en la hidrodinámica de los vientos producidos por cúmulos estelares.

El objetivo principal de esta tesis es desarrollar un método semi-analítico para resolver el sistema de ecuaciones hidrodinámicas unidimensionales tomando en cuenta el enfriamiento radiativo del gas y obtener la distribucón de las variables hidrodinámicas (velocidad de expansión, temperatura del viento, densidad numérica de partículas, presión térmica y presión de empuje) para vientos producidos por cúmulos estelares con una distribución de densidad estelar más realista.

Para una distribución de densidad estelar homogénea, el punto singular, *i.e.* el radio en el que el viento pasa de ser subsónico a supersónico, se encuentra ubicado forzosamente sobre la superficie del cúmulo estelar (Chevalier & Clegg, 1985). Sin embargo, para una distribución de densidad estelar exponencial, no existe tal superficie del cúmulo estelar y por consiguiente la posición del punto singular debe ser calculada.

Es por esto que en esta tesis, se propone un procedimiento que permite calcular la ubicacón del punto singular de manera autoconsistente. El resultado principal de este cálculo es que en el régimen de viento quasi-adiabático, el punto singular se encuentra ubicado siempre a cuatro veces el radio de escala desde el centro del cúmulo estelar. Además, la presión de empuje es igual a la presión térmica a un radio tres veces mayor al radio de escala del cúmulo estelar. Por otra parte, en el régimen de viento con enfriamiento catastrófico, la temperatura decae de manera rápida a distancias muy cercanas al punto singular y éste deja de encontrarse a cuatro veces el radio de escala y comienza a acercarse al centro del cúmulo estelar.

Acknowledgment

First and foremost, I would like to thank God, the Omnipotent, for having made everything possible by giving me strength and courage to do this work and all His work in my life. ***::DEO GRATIAS::***.

I am heartily thankful to my Parents, Enrique Javier (*Requiescat in Pace*) & María Elena, and my Brother, Francisco Enrique, who have gave me their unconditional love and tireless support during all my life. I am deeply indebted to my sweet Karla Evelyn for her invaluable love.

My sincere thanks to my advisors, Sergiy Silich and Guillermo Tenorio-Tagle, whose encouragement, guidance and constant support from the initial to the final level enabled me to develop an understanding of the subject.

I am also indebted to my examiners: ——————————————————————————-. They have also contributed to this success.

It is difficult to overstate my appreciation to Prof. Wolfgang Steffen,

who first brought me into the world of research and with whom I began to learn about stellar winds.

I would like to thank the CONACyT (Consejo Nacional de Ciencia y Tecnología). Without their scholarship (No. 335715), this thesis would not have been possible. This study was also supported by CONACYT research grant 131913.

Last, but no least, I offer my regards and blessings to all of those who supported me in any respect during the completion of my Master's degree: Francisco Soto Eguibar, Jordán Lima, Olga Vega & Daniel Rosa, Manuel Corona, Miguel Chávez, José Ramón Valdés, Filiberto Hueyotl, Fernando Cruz, Bernardo Guerrero & Jesús Reyes. I have an urge to individually thank all of my friends which, from my childhood until graduate school, have shared life with me. However, because the list might be too long and by fear of leaving someone out, I will simply say thank you very much to you all.

Ad Maiorem Dei Gloriam. A mis Padres, Enrique Javier † y María Elena, a mi Hermano, Francisco Enrique, a mi Sobrino y Cuñada, Luis Ángel y Karolina, y a Karla Evelyn.

List of Symbols

The following table lists the symbols that are used throughout this thesis.

L_{sc}	The star cluster total mechanical luminosity.
M_{sc}	The star cluster total mass.
r	The distance to the star cluster center.
R_c	The star cluster core radius.
R_k	The star cluster core radius for King models.
R_{HM}	The star cluster half-mass radius.
$R_{_{RAM}}$	The distance at which the ram pressure is equal to the thermal pressure.
R_{sp}	The radius of the singular point.
ρ_*	The stellar mass density.
ρ_{*k}	The stellar mass density for King models.
ρ_w	The wind density.
n_w	The wind number density.
$u_{A\infty}$	The adiabatic wind terminal velocity.
v_∞	The wind terminal velocity.
v_{esc}	The star cluster escape velocity.
c_s	The local sound speed.
c_c	The central value of the sound speed.
c_{sp}	The sound speed at the singular point.
u_w	The wind velocity.
u_{sp}	The wind velocity at the singular point.
T_w	The wind temperature.
T_c	The central temperature.
T_{wc}	The central temperature which corresponds to the wind solution.
T_{sp}	The wind temperature at the singular point.
T_c^{max}	The adiabatic wind central temperature.
P_w	The wind thermal pressure.
Z	The gas metallicity.
$\mathrm{Z}_\odot$	The solar metallicity.

q_m	The mass deposition rate per unit volume.
q_e	The energy deposition rate per unit volume.
Q	The cooling rate.
Q_c	The central value of the cooling rate.
Λ	The cooling function.
γ	The ratio of specific heats.
U	The star cluster gravitational potential.
G	The gravitational constant.
$M_\odot$	The solar mass.
k_B	The Boltzmann constant.
μ_{tot}	The mean mass per particle.
μ_{ion}	The mean mass per particle of ionized gas.
m_H	The proton mass.

Contents

Chapter 1

Introduction

Super star clusters (SSCs) are high-density coeval young stellar systems which contain between $10^5 - 10^7$ $M_\odot$ within a radius of few parsecs ($\sim 1 - 10$ pc) (Whitmore, 2000). They are usually found in systems with an intense mode of star formation, such as the most luminous HII and starburst galaxies (Meurer et al., 1995; O'Connell et al., 1994; Whitmore & Schweizer, 1995; Johnson et al., 2000, and references therein).

SSCs drive powerful winds formed by the thermalization of the kinetic energy supplied by massive stars and high velocity supernova explosions. Moreover, it is nowadays recognized that most of stars, if not all of them, are formed in clustered environments (Lada & Lada, 2003) resulting in a combined effect of winds of many stars. This combined effect can drive galactic-scale winds which affect the evolution of the host galaxy itself and its surroundings (Heckman et al., 1990).

In sections 1.1 and 1.2 I briefly review the main observations of star clusters and the major contributions regarding the hydrodynamics of star cluster driven winds. In section 1.3, I present the objectives of this thesis.

1.1 Observations of super star clusters

SSCs were first identified by Arp & Sandage (1985) when they were studying the morphology of what appear to be two blue knots in NGC 1569 (cf. Figure 1.1) and by Melnick et al. (1985) with a similar object in NGC 1705. A prominent example of a young compact cluster is the central object of the Tarantula Nebula (30 Doradus),

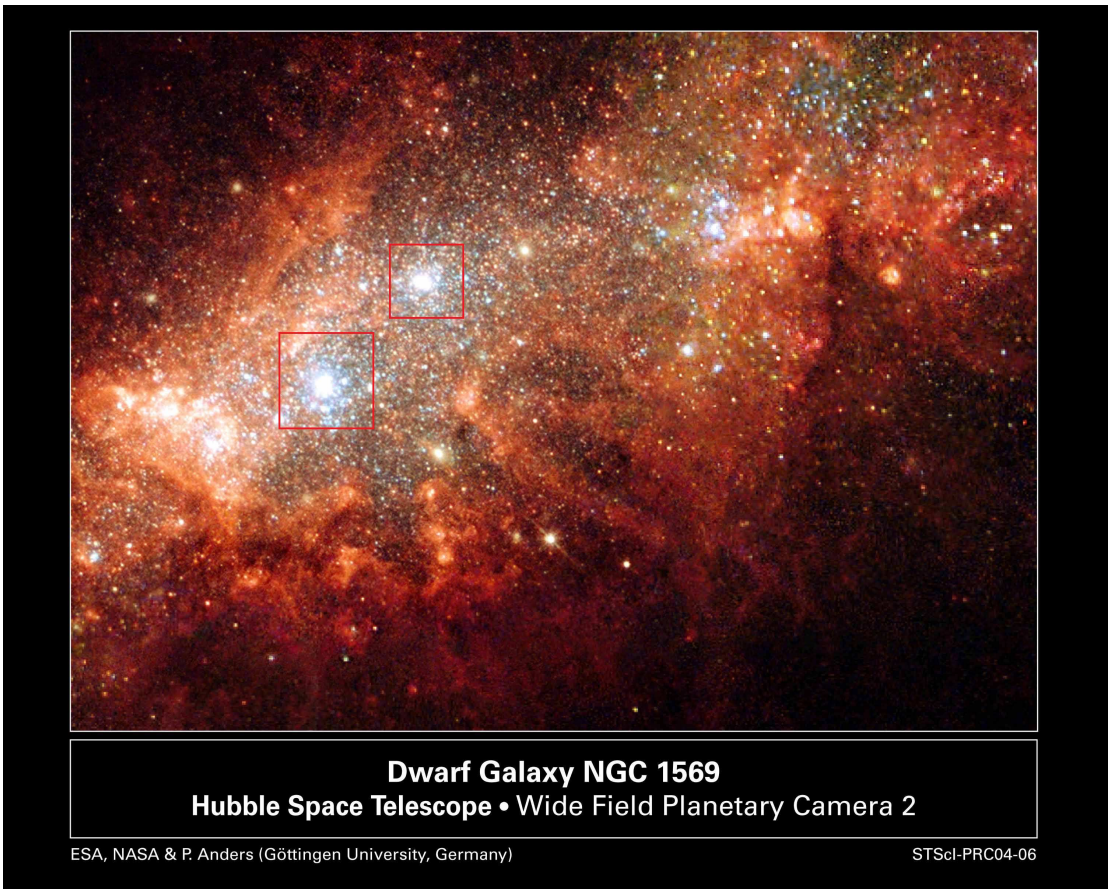

Figure 1.1: HST image of NGC 1569. The image exhibits two prominent blue star clusters experiencing intense episodes of star formation. Image credit: NASA, ESA & P. Anders.

R136, whose core was once believed to be an individual supermassive star of at least $2000\ M_{\odot}$. Weigelt & Baier (1985), using a holographic speckle interferometry technique, unambiguously identified for the first time what they described to be at least eight individual stars in R136 (cf. Figure 1.2).

The advent and implementation of the Hubble Space Telescope (HST) and its ability to resolve individual stars in nearby galaxies gave the opportunity for the confirmation of the existence of many extragalactic super star clusters. The undoubtedly proof came from Holtzman et al. (1992), who discovered a population of many SSCs within 5 kpc of the nucleus of NGC 1275. Shortly after, it was confirmed that starbursts are in fact composed by many SSCs. For example, the local starburst M82 contain ~ 653 star clusters of which ~ 260 are located within the central 450 pc (Melo et al., 2005; Mayya et al., 2008).

Figure 1.2: HST image of the R136 Cluster in the center of 30 Doradus. R136a was originally thought to be a supermassive star. Image credit: HST/NASA/ESA.

The typical sizes of SSCs (also called young star clusters) of about $\sim 1 - 10$ pc, resemble those of the old Galactic globular clusters. Estimates of cluster ages have shown that SSCs are usually older than their crossing times, indicating that they are gravitationally bound (McCrady et al., 2003).

The radial profiles of young star clusters are best reproduced by King models (King, 1962; Mengel et al., 2002) derived for globular clusters. It has been suggested that at least a small fraction of SSCs could survive and eventually become nowadays globular clusters (Billett et al., 2001; Portegies Zwart et al., 2010).

1.2 The Star Cluster Driven Wind Theory

Star cluster winds are important in interstellar astrophysics because they affect the evolution of the surrounding interstellar medium, enrich it with the products of massive stars evolution and may result in triggering subsequent star formation.

The physical processes which drive star cluster winds are different from those which drive winds from individual stars. Winds from individual stars are formed due to radiation pressure absorbed in the outer layers of stars. Instead, Chevalier & Clegg (1985,

hereafter CC85) proposed that star cluster winds are formed due to the efficient thermalization of the kinetic energy caused by random collisions of gas ejected by supernova explosions and stellar winds. This produces a large central overpressure that allows the reinserted matter to accelerate and form strong outflows, the star cluster winds.

CC85 presented an analytical solution for winds driven by starbursts with radius R_{sc} and uniform mass and energy deposition rates. Cantó et al. (2000) compared the CC85 analytic predictions with winds generated by discrete stars (with a mean separation of 0.1 pc) assuming much larger ranges of temperatures and densities than the CC85 model. They also carried out numerical simulations and found that the analytic solution and the numerical results are in a reasonable agreement. These adiabatic models predict the existence of extended X-ray envelopes that could be observationally detected.

In these models, the expansion velocity grows rapidly from zero km s^{-1} at the star cluster center to the sound speed at the star cluster surface R_{sc}. Thus, inside the star cluster, the density, pressure and temperature of the wind remain almost uniform. However, outside R_{sc}, the hydrodynamical properties of the resultant wind outflow (the run of density, temperature and expansion velocity), asymptotically approach $\rho_w \sim r^{-1/2}$, $T_w \sim r^{-4/3}$ and $u_w \sim u_{A\infty}$, where $u_{A\infty}$ is the adiabatic wind terminal velocity.

Silich et al. (2004) presented a self-consistent stationary semi-analytic solution for spherically symmetric winds driven by massive homogeneous star clusters which includes radiative cooling. They found that radiative cooling may *change significantly the temperature distribution of the wind* in the case of very massive and compact star clusters. They found a threshold line in the plane $L_{sc}\ vs.\ R_{sc}$ (where L_{sc} is the mechanical luminosity), above which the stationary wind solution is inhibited.

Additionally, they discussed the solution topology for the hydrodynamic equations. In their model, there are three possible types of integral curves corresponding to different possible positions of the singular point with respect to the star cluster surface: the stationary wind solution in which the singular point is located at the star cluster surface and the flow is subsonic inside and supersonic outside the star cluster. The breeze solution in which the central temperature is smaller than in the stationary wind solution; the maximum value of the outflow velocity is shifted outside the star cluster and the flow is subsonic everywhere. The unphysical double valued solution in which the central temperature is larger than in the stationary wind case.

Tenorio-Tagle et al. (2007) confirmed with 1D numerical simulations the location of the threshold line found in Silich et al. (2004) in the case of a homogeneous distribution of stars and found solutions above that threshold line. In that case, the singular point remains fixed at the star cluster surface and the stagnation point (R_{st}; the point where the expansion velocity vanishes), moves from the star cluster center towards the star cluster surface when more massive and compact clusters are considered. This is because densest regions result in an immediate loss of pressure and of the outward pressure gradient.

Rodríguez-González et al. (2007) proposed a non-radiative analytic wind model for star cluster winds with a power-law stellar density distribution, $\rho_* \propto R^{\alpha}$, where α is a constant and R the distance to the star cluster center. They introduced a truncation radius, R_c, to impose a star cluster surface and assumed that the singular point is located exactly at $R = R_c$. Thus they compared the analytic star cluster wind solutions with 3D numerical simulations and obtained a good agreement.

Ji et al. (2006), solved one-dimensional hydrodynamic equations numerically and obtained steady-state adiabatic wind solutions for star clusters with an exponential stellar density distribution $\rho_* \propto \exp(-r/R_c)$, where r is the distance to the star cluster center and R_c the star cluster core radius. They asseverated that the location of the singular point depends on the stellar density distribution alone. This model can be directly compared to the solution presented in this thesis.

These results have significantly improved the idealized CC85 model. In this thesis, the hydrodynamic model is refined by assuming a more realistic exponential stellar density distribution and also by calculating the position of the singular point self-consistently taking into account the effects of radiative cooling.

1.3 Aim of the Thesis

The aim of this thesis is to develop a semi-analytic method to solve the steady-state hydrodynamic equations for star cluster winds. The method takes into account the effects of radiative cooling and a non-homogeneous stellar density distribution.

The main differences with previous works in the field are

- There is no star cluster surface since the exponential profile extends to infinity. Instead a star cluster core radius is used as an input parameter.
- The position of the singular point is calculated self-consistently.
- The initial and boundary conditions are derived using a semi-analytical approach.
- The effects of radiative cooling are taken into account.
- The semi-analytic method described in this thesis is not limited to an exponential stellar density distribution. It can be easily extended to other stellar density distributions.

1.4 Structure of the Thesis

The thesis is organized as follows:

In Chapter 2, the star cluster model is presented. The motivations for using an exponential stellar density distribution are outlined. Additionally, I obtain the relations between the star cluster core radius, and the half-mass radius for star clusters with a King stellar density distribution and compare them to that obtained in the case of an exponential stellar density distribution.

In Chapter 3, the model for winds driven by SSCs with an exponential distribution of stars is described. I follow the original idea of Chevalier & Clegg (1985), which basically suggests that all the mechanical energy deposited by massive stars and supernova explosions is transformed into thermal energy via random collisions of nearby stellar winds and supernova ejecta. The main hydrodynamic equations are adapted to the case when stars are exponentially distributed. Then, they are combined and presented in a suitable form for numerical integration.

In Chapter 4, the semi-analytic radiative method is described and applied to the case of an exponential distribution of stars. Here, I discuss the topology of the integral curves and the initial and boundary conditions which allow one to select the proper solution from the infinite number of integral curves.

In Chapter 5, the results of the calculations are discussed. Firstly I verify the method using the results obtained by Ji et al. (2006). Then I compare models with different

input parameters to a reference model. The impact of radiative cooling is then discussed emphasizing the main differences with adiabatic and quasi-adiabatic wind regimes.

Finally, in Chapter 6, I briefly summarize the main results and outline a number of possible extensions to this work.

Chapter 2

The Star Cluster Model

In this chapter the star cluster model is formulated. In contrast with most previous works in the field, the stars are not homogeneously distributed inside a star cluster surface but follow an exponential distribution. In section 2.1, I obtain the relations between the star cluster core radius, and the half-mass radius for star clusters with a King stellar density distribution and compare them to that obtained in the case of an exponential stellar density distribution. Additionally,, the star cluster escape velocity is compared, in section 2.2, to the sound speed in order to justify why I do not take into consideration the gravitational pull of the star cluster and tidal forces. In section 2.3 the motivations for using an exponential stellar density distribution are outlined.

2.1 Star Cluster Model

A young (≤ 40 Myr), compact stellar cluster with total mass M_{sc} and no-time dependent parameters is considered.

It is also assumed that

- The star cluster is spherically symmetric;
- The stellar mass density distribution is an exponential function with respect to the distance to the star cluster center

$$\rho_*(r) = \rho_{*o} e^{-r/R_c} \, , \tag{2.1}$$

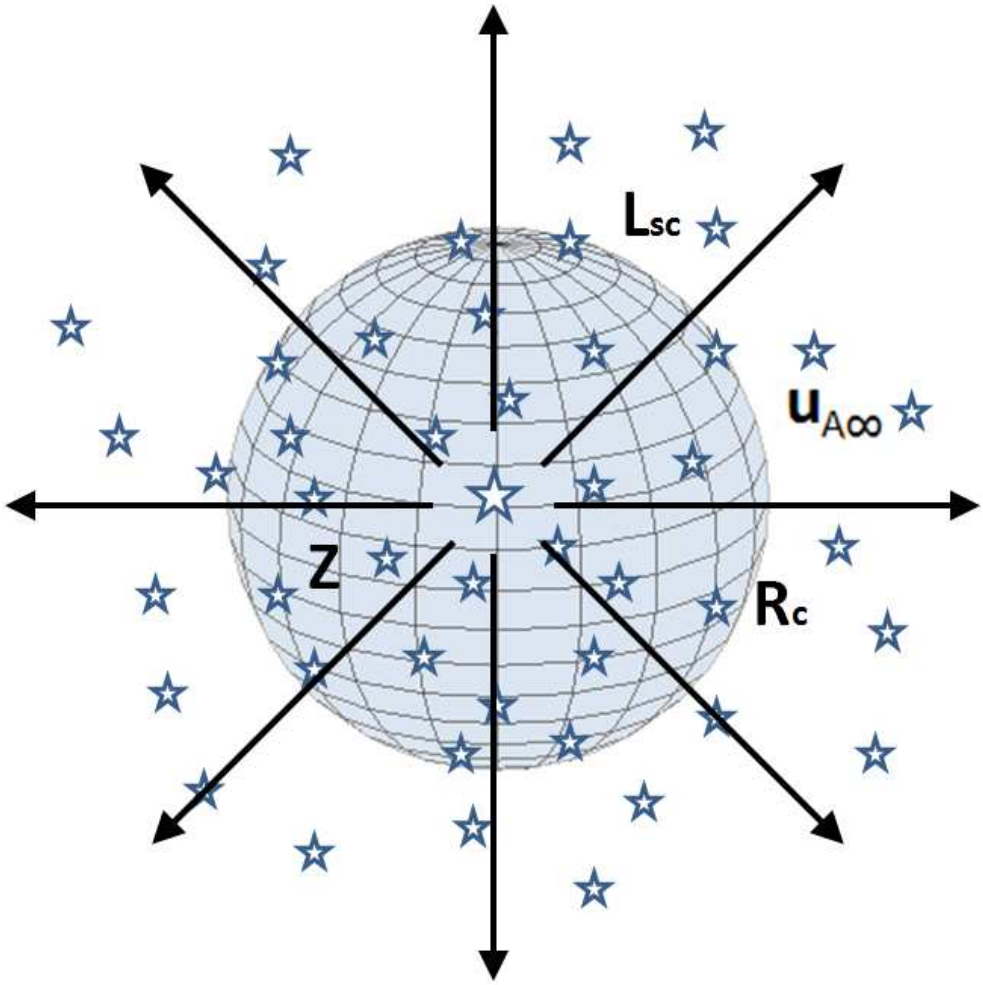

Figure 2.1: Schematic representation of the model. The volume inside the sphere represents the core of the star cluster for a non-homogeneous distribution of stars.

where R_c is the star cluster core radius and ρ_{*o} is the stellar mass density at the star cluster center;

- The mechanical luminosity L_{sc} is related to the total mass of the star cluster M_{sc} (cf. Leitherer et al., 1999) as

$$L_{sc} \approx 3 \times 10^{40} \left(\frac{M_{sc}}{10^6 M_\odot} \right) \text{ erg s}^{-1} ;$$

- The gravitational pull from the star cluster and tidal forces are negligible and thus a tidal radius is not considered so the star cluster extends to infinity (cf. Figure 2.1).

The two parameters, L_{sc} and $\dot{M}_{sc}$, are related by the equation

$$L_{sc} = \frac{1}{2}\dot{M}_{sc}u_{A\infty}^2 \tag{2.2}$$

where $u_{A\infty}$ is the adiabatic wind terminal velocity. I will use $u_{A\infty}$ as the input parameter of the model instead of $\dot{M}_{sc}$ for all the calculations.

The mass $M(r)$ at any distance from the star cluster center can be found by integration

$$M(r) = 4\pi \int_0^r \rho_*(r) r^2 dr = M_{sc}\left[1 - \left(1 + \frac{r}{R_c} + \frac{1}{2}\frac{r^2}{R_c^2}\right) e^{-r/R_c}\right] , \tag{2.3}$$

where the total mass of the star cluster is

$$M_{sc} \;=\; \int_0^\infty 4\pi r^2 \rho_*(r) dr = 8\pi\rho_{*o}R_c^3 \, . \tag{2.4}$$

Note that terms in the bracket, $\left(1 + \frac{r}{R_c} + \frac{1}{2}\frac{r^2}{R_c^2}\right)$, coincide with the first three terms of the Taylor series around zero for the exponential function e^{r/R_c}.

The stellar mass density at any distance to the star cluster center is then

$$\rho_*(r) = \frac{M_{sc}}{8\pi R_c^3} e^{-r/R_c} \, . \tag{2.5}$$

The difference between the exponential and homogeneous distributions is that in the exponential case the star cluster does not have an edge. Nevertheless, the total mass of the star cluster is finite.

Equation (2.3) allows to calculate the relation between the half-mass radius R_{HM} and the star cluster core radius

$$R_{HM}/R_c \approx 2.66 \, , \tag{2.6}$$

Thus the half mass radius is larger than the star cluster core radius by a factor of 2.66. This relation is important in order to compare models with different stellar density distributions whe the star clusters have the same half-mass radius.

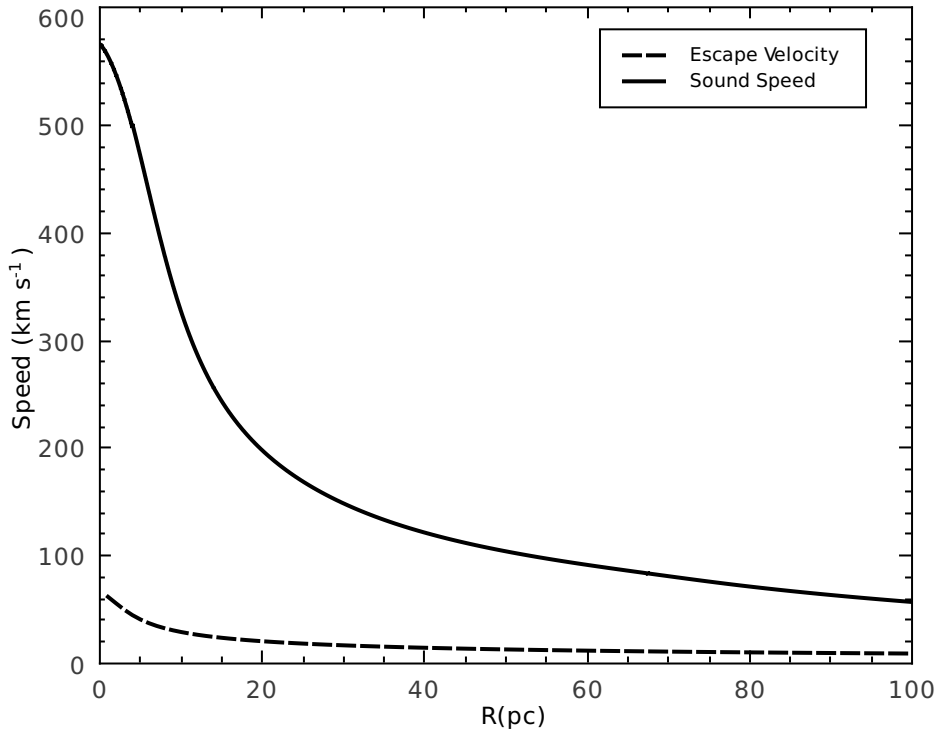

Figure 2.2: Comparison between the adiabatic sound speed (solid line) and the escape velocity (dashed line) of the star cluster. The total mass of the star cluster is assumed to be $M_{sc} = 10^6$ M$_\odot$, the adiabatic wind terminal velocity is $u_{A\infty} = 1000$ km s^{-1} and the star cluster core radius is $R_c = 1$ pc.

2.2 The Star Cluster Escape Velocity

In the case of an extended star cluster, the escape velocity v_{esc} is defined by the equation (Clarke & Carswell, 2007)

$$v_{esc}^2 = -2U = 2G \int_r^\infty \frac{M(r)dr}{r^2} \,, \tag{2.7}$$

where U is the gravitational potential of the star cluster and G is the gravitational constant. Substituting equation (2.3) into (2.7), the escape velocity from the star cluster with an exponential stellar density distribution is then

$$v_{esc}^2 \;=\; 2GM_{sc}\left[-\frac{1}{r} + \frac{e^{-r/R_c}}{r} + \int_r^\infty \frac{e^{-r/R_c}}{rR_c} - \int_r^\infty \frac{e^{-r/R_c}}{rR_c} + \frac{e^{-r/R_c}}{2R_c}\right]\Bigg|_r^\infty \tag{2.8}$$

Thus the escape velocity for star clusters with an exponential stellar density distribution is then

$$v_{esc} = \sqrt{2GM_{sc}\left[\frac{1}{r}\left(1 - e^{-r/R_c}\right) - \frac{e^{-r/R_c}}{2R_c}\right]} \tag{2.9}$$

I do not take into consideration the gravitational pull of the star cluster and tidal forces because the sound speed of the shocked gas at a given radius is usually much higher than the corresponding star cluster escape velocity. Figure 2.2 compares the sound speed in the star cluster wind with the star cluster escape velocity when the mass of the star cluster is $M_{sc} = 10^6$ M$_\odot$, the adiabatic wind terminal velocity is $u_{A\infty} = 1000$ km s^{-1} and the star cluster core radius is $R_c = 1$ pc.

2.3 An Exponential *versus* a King Stellar Density Distribution

Mengel et al. (2002) observed a sample of super star clusters in the *Antennae* galaxies and found that the best fitting model for the light profiles of star clusters is a King model (King, 1962). Then they assumed that the light distribution follows the mass distribution and concluded that the effective radii of star clusters are approximately 4 pc, similar to what Whitmore et al. (1999) estimated as the average radius of the stellar clusters in the *Antennae*.

I adopt exponential profiles instead of King profiles because a King profile implies an infinite total mass if one does not account for a tidal radius. This problem does not occur if one assumes an exponential profile. Moreover, the exponential profile is algebraically easier to deal with. Note that the model presented in this work can be easily extended to the case of modified King profiles which have been proposed by Elson et al. (1987, hereafter EFF)

$$\rho_*(r) = \frac{\rho_{*o}}{\left[1 + \left(\frac{r}{R_k}\right)^2\right]^\alpha} \tag{2.10}$$

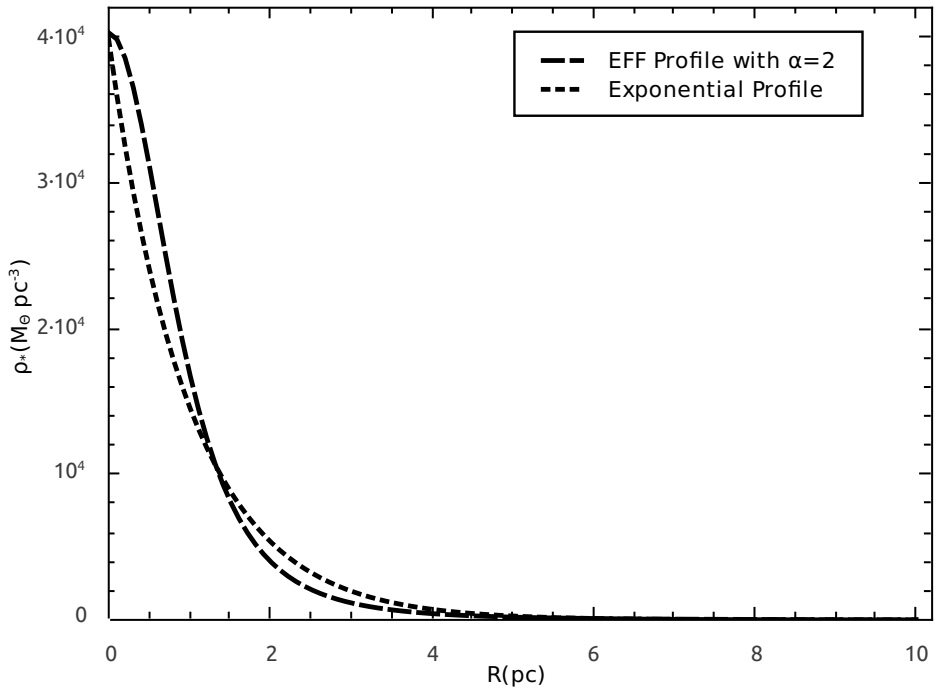

Figure 2.3: Comparison between a modified King profile with index $\alpha = 2$ (EFF) and an exponential profile for the stellar density distribution.

where R_k is the star cluster core radius for the modified King model. Note that if α is ≤ 1, the total mass of the star cluster is infinite. If $\alpha > 1$, the total mass of the star cluster is finite. These profiles provide a good fit to the star clusters in the Large Magellanic Cloud (Larsen et al., 2004).

The total mass of the star cluster in the case of a modified King Profile with index $\alpha = 2$ is

$$M_{sc} = 4\pi\rho_{*ko}\int_0^\infty \frac{r^2}{\left[1+\left(\frac{r}{R_k}\right)^2\right]^2}dr = \pi^2\rho_{*ko}R_k^3\,, \tag{2.11}$$

where ρ_{*ko} is the central stellar mass density of a modified King profile. If it is assumed that they lead to the same total star cluster mass, M_{sc}, one can obtain the relation between an exponential and a modified King profile core radii. In this case, equations (2.4) and (2.11), lead to the relation

$$R_k = \sqrt{\frac{8\rho_{*o}}{\pi\rho_{*ko}}} R_c \, . \tag{2.12}$$

When the central stellar mass densities, ρ_{*o} and ρ_{*ko} are also equal, equation (2.12) yields

$$R_k = \sqrt{\frac{8}{\pi}} R_c \approx 1.365 R_c. \tag{2.13}$$

Thus in the case of the modified King profile with $\alpha = 2$, the star cluster core radius R_k is larger than in the exponential case within a factor of $R_k \approx 1.365 R_c$. Figure 2.3 compares the adopted exponential and modified King profiles in the case when the total mass of the star cluster is $M_{sc} = 10^6 \mathrm{M}_\odot$.

Chapter 3

The Star Cluster Wind Model

In this chapter, the model for winds driven by SSCs with an exponential distribution of stars is constructed. The main hydrodynamic equations are adapted to the case when stars are exponentially distributed. Then, they are combined and presented in a suitable form for numerical integration.

3.1 Main Hydrodynamic Equations

Steady state spherically symmetric hydrodynamic equations which take into consideration the energy and mass continuously deposited to the flow (see, for example Johnson & Axford, 1971; Chevalier & Clegg, 1985; Cantó et al., 2000; Silich et al., 2004; Ji et al., 2006, and references therein) are

$$\frac{1}{r^2}\frac{d}{dr}(\rho_w u_w r^2) \;=\; q_m \,, \tag{3.1}$$

$$\rho_w u_w \frac{du_w}{dr} = -\frac{dP_w}{dr} - q_m u_w \,, \tag{3.2}$$

$$\frac{1}{r^2}\frac{d}{dr}\left[\rho_w u_w r^2 \left(\frac{1}{2}u_w^2 + \frac{\gamma}{\gamma-1}\frac{P_w}{\rho_w}\right)\right] \;=\; q_e - Q \,. \tag{3.3}$$

where P_w, u_w, and ρ_w are the thermal pressure, the velocity and the density of the thermalized matter, $\gamma = 5/3$ is the ratio of specific heats, $Q = n_w^2 \Lambda(Z,T)$ is the cooling rate, n_w is the wind number density and $\Lambda(Z,T)$ is the cooling function which depends on the gas metallicity Z and temperature T_w (Raymond et al., 1976) (cf. Figure 3.1). The last term in the momentum conservation equation (3.2), $q_m u_w$, is negative because it is assumed that the injected material has zero momentum.

The mass and energy deposition rates per unit volume, q_m and q_e are

$$q_m = q_{mo} e^{-r/R_c} , \qquad q_{mo} = \frac{\dot{M}_{sc}}{8\pi R_c^3} , \tag{3.4}$$

and

$$q_e = q_{eo} e^{-r/R_c} , \qquad q_{eo} = \frac{L_{sc}}{8\pi R_c^3} . \tag{3.5}$$

In the case of a completely ionized plasma, the wind number density can be expressed as $n_w = \dfrac{\rho_w}{\mu_{tot}}$, where $\mu_{tot} = \frac{14}{23} m_H$ is the mean mass per particle and m_H is the proton mass.

Four cluster parameters completely define the solution in the case of an exponential stellar density distribution: the mechanical luminosity, the adiabatic wind terminal velocity, the gas metallicity and the characteristic length scale for the stellar mass distribution, or star cluster core radius.

The integration of the mass conservation equation (3.1) yields

$$\begin{aligned} \rho_w u_w r^2 &= \int \frac{\dot{M}_{sc}}{8\pi R_c^3} r^2 e^{-r/R_c} dr \\ &= \frac{\dot{M}_{sc}}{8\pi R_c^3} e^{-r/R_c} \left[-2R_c^3 - 2R_c^2 r - R_c r^2 \right] + C . \end{aligned} \tag{3.6}$$

where C is the integration constant. If the wind central density is finite, then

$$C = 2 q_{mo} R_c^3 . \tag{3.7}$$

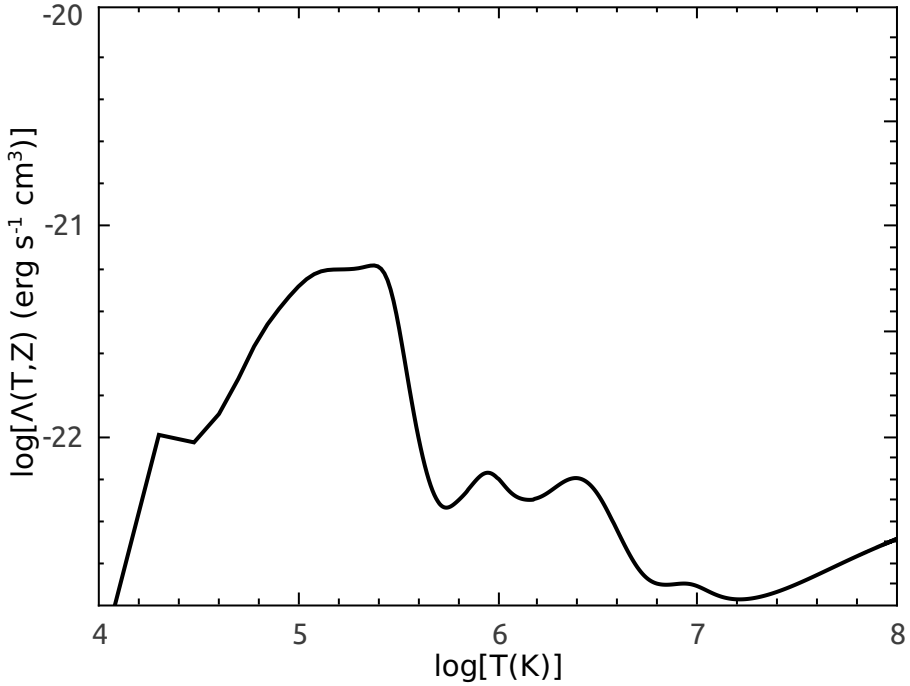

Figure 3.1: The Cooling Function for solar metallicity.

Thus in the exponential case, the integration constant is not zero as in the homogeneous case. The density distribution in the flow is then

$$\rho_w = \frac{2q_{mo}R_c^3}{u_w r^2}\left[1-\left(1+\frac{r}{R_c}+\frac{1}{2}\frac{r^2}{R_c^2}\right)e^{-r/R_c}\right]. \tag{3.8}$$

Substituting equation (3.8) into equation (3.2), one can obtain

$$\frac{2q_{mo}R_c^3}{r^2}\left[1-\left(1+\frac{r}{R_c}+\frac{1}{2}\frac{r^2}{R_c^2}\right)e^{-r/R_c}\right]\frac{du_w}{dr} = -\frac{dP_w}{dr}-q_m u_w. \tag{3.9}$$

Solving the above equation for the derivative of the thermal pressure one obtains

$$\frac{dP_w}{dr} = -\frac{2q_{mo}R_c^3}{r^2}\left[1-\left(1+\frac{r}{R_c}+\frac{1}{2}\frac{r^2}{R_c^2}\right)e^{-r/R_c}\right]\frac{du_w}{dr}-q_m u_w. \tag{3.10}$$

Calculating explicitly the derivative in the energy conservation (3.3) one can obtain

$$\begin{aligned}\frac{1}{r^2}\frac{d}{dr}\left[\rho_w u_w r^2\left(\frac{1}{2}u_w^2+\frac{c_s^2}{\gamma-1}\right)\right] &= q_m\left\{\frac{u_w^2}{2}+\frac{c_s^2}{\gamma-1}\right\}+\rho_w u_w\left\{u_w\frac{du_w}{dr}+\frac{d}{dr}\frac{c_s^2}{\gamma-1}\right\}\\ &= q_e-Q, \end{aligned} \tag{3.11}$$

where c_s is the local sound speed given by $c_s^2=\dfrac{\gamma k_B}{\mu_{ion}}T_w=\gamma\dfrac{P_w}{\rho_w}$, k_B is the Boltzmann constant and $\mu_{ion}=\frac{14}{11}m_H$ is the total mean mass per particle of the ionized gas in terms of the hydrogen mass.

Combining equation (3.11) with equations (3.1), (3.8) and (3.2), one can obtain

$$\begin{aligned} q_e-Q &= \rho_w u_w^2\frac{du_w}{dr}+\frac{u_w^2}{2}q_m\\ &+ \frac{\gamma}{\gamma-1}\left\{\rho_w\left(\frac{c_s^2}{\gamma}-u_w^2\right)\frac{du_w}{dr}-q_m u_w^2+\frac{4q_{mo}R_c^3}{r^3}\frac{P_w}{\rho_w}\left[1-\left(1+\frac{r}{R_c}+\frac{1}{2}\frac{r^2}{R_c^2}\right)e^{-r/R_c}\right]\right\}. \end{aligned} \tag{3.12}$$

When one multiplies both sides of equation (3.12) by $(\gamma-1)$, one can express the change of the wind velocity with respect to the distance to the star cluster center as

$$\frac{du_w}{dr} = \frac{(\gamma-1)(q_e-Q)-\dfrac{4q_{mo}R_c^3c_s^2}{r^3}(1-e^{-r/R_c})+q_m\left[\dfrac{u_w^2}{2}(\gamma+1)+4\dfrac{R_c^3}{r^3}\left(\dfrac{r}{R_c}+\dfrac{1}{2}\dfrac{r^2}{R_c^2}\right)c_s^2\right]}{\rho_w(c_s^2-u_w^2)}. \tag{3.13}$$

Equations (3.8), (3.10) and (3.13) are more suitable for numerical integration than equations (3.1), (3.2) and (3.3). In the next chapter, the methodology for solving them is presented.

Chapter 4

Methodology for solving the Boundary-Value Problem

In this chapter, a semi-analytic method for solving the hydrodynamic equations formulated in the preceding chapter is developed. Firstly, in section 4.1 I discuss the topology of the possible solutions of the differential equations (3.10) and (3.13). Then in sections 4.2 and 4.3 I discuss the initial and boundary conditions which allow one to select the proper solution from the infinite number of integral curves. The proper solution is the only solution which passes through the singular point, *i.e.* the point at which the wind becomes supersonic. The procedure for solving the problem uses three integrations: one from the star cluster center outwards, one from the singular point inwards and one starting at the singular point outwards.

4.1 Topology of the Integral Curves

Equations (3.10) and (3.13) have an infinite number of solutions, each one selected by the value of the central temperature. In order to select the proper integral curve from the infinite number of possible solutions it is useful to examine the solution topology. Different central temperatures lead to three possible types of integral curves (cf. Figure 4.1).

- The wind solution is the only solution which starts subsonic, goes through the

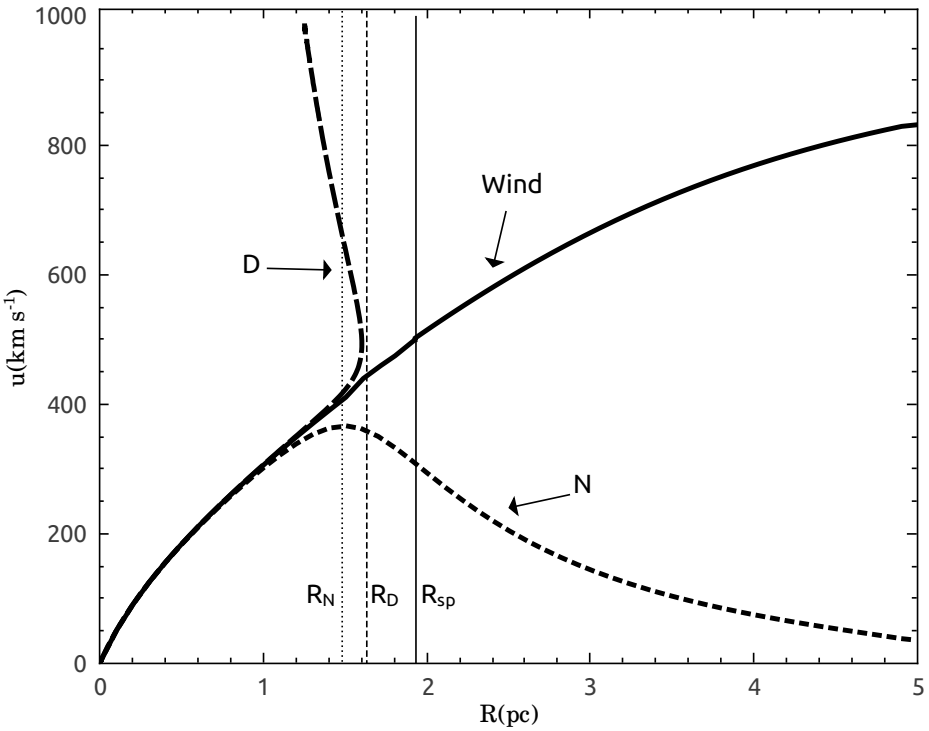

Figure 4.1: Types of integral curves for the differential equation (3.13). The solid line corresponds to the wind solution. The thin dashed line corresponds to the N-type solution and the thick dashed line corresponds to the D-type solution.

singular point, R_{sp}, where the numerator and the denominator of equation (3.13) change their sign simultaneously, and then reaches supersonic values farther outwards. Notice, that the central temperature which leads to the wind solution must be selected with high accuracy.

- The N-type solution occurs when the central temperature is lower than in the wind solution. In this case, the solution remains subsonic everywhere. The change of sign in equation (3.13) only takes place in the numerator. The outflow velocity reaches its maximum value at a radius R_N from the star cluster center and then decreases with increasing radius from there off.

- The D-type solution is an unphysical double-valued solution which occurs when the central temperature is greater than that for the wind solution. In this case

only the denominator of equation (3.13) changes its sign. In order to obtain this solutions, one has to rewrite equation (3.13), using u_w instead of r as the independent variable.

As shown in Figure 4.1, in the case of star clusters with an exponential stellar density distribution, the singular point R_{sp} is located ahead of R_D and R_N. Thus, both R_D and R_N converge to R_{sp} from the left when the central temperature goes to the correct wind value. In order to select the central temperature T_{wc} which corresponds to the wind solution, one can implement an iteration procedure. The procedure is as follows

1. Integrate equations (3.10) and (3.13) using three different trial central temperatures T_1, T_2 and $T_{12} = (T_1 + T_2)/2$, with $T_1 < T_{wc} < T_2$, and check for changes of sign in the numerator, N, and the denominator, D, of equation (3.13). There are now 2 possibilities

   (a) If integrations with the central temperatures T_1 and T_{12} change the sign of the numerator and integration with T_2 changes the sign of the denominator, then T_1 must be replaced with T_{12}.

   (b) If integrations with the central temperatures T_{12} and T_2 change the sign of the numerator and integration with T_1 changes the sign of the denominator, then T_2 must be replaced with T_{12}.

2. Repeat iterations in the halved interval. The iteration process must be continued until the accuracy Δ for locating the singular point is achieved. This accuracy is given by

$$\Delta = \frac{\sqrt{(R_{SPA} - R_N)^2 + (R_{SPA} - R_D)^2}}{R_{SPA}} \,, \tag{4.1}$$

   where $R_{SPA} = (R_N + R_D)/2$. The accuracy Δ is usually taken within the range $\sim 10^{-4} - 10^{-3}$.

4.2 The Initial Conditions at the star cluster center

In order to start integrations, one has to select the velocity u_w, the density ρ_w (or equivalently n_w) and the temperature T_w at the star cluster center.

It looks like equations (3.8) and (3.13) have a singularity at the star cluster center. However, this is not the case. Indeed, using the L'Hôpital's rule and the condition that the wind central density must be finite, one can obtain the following limits

$$\lim_{r\to 0} u_w = \frac{2q_{mo}}{\rho_{wo}} \lim_{r\to 0} \frac{R_c^3}{r^2}\left[1-\left(1+\frac{r}{R_c}+\frac{1}{2}\frac{r^2}{R_c^2}\right)e^{-r/R_c}\right] = 0\,. \tag{4.2}$$

$$\begin{aligned}\lim_{r\to 0}\frac{du_w}{dr} &= \lim_{r\to 0}\frac{(\gamma-1)(q_e-Q)-\frac{4q_{mo}R_c^3c_s^2}{r^3}(1-e^{-r/R_c})+\frac{4q_mR_c^3}{r^3}\left(\frac{r}{R_c}+\frac{1}{2}\frac{r^2}{R_c^2}\right)c_s^2}{\rho_w c_s^2} \\ &= \frac{(\gamma-1)(q_{eo}-Q_c)-\frac{2}{3}q_{mo}c_c^2}{\rho_{wo}c_c^2}\,,\end{aligned} \tag{4.3}$$

where q_{eo} and Q_c are the central values for the energy deposition rate per unit volume and the cooling rate, respectively. Besides this, one can obtain the relation between the wind central density and the wind central temperature. Indeed the energy conservation equation (3.11) leads to the relation

$$q_e - Q = q_m\left[\frac{u_w^2}{2}+\frac{c_s^2}{\gamma-1}\right]+\rho_w u_w\left[u_w\frac{du_w}{dr}+\frac{d}{dr}\frac{c_s^2}{\gamma-1}\right]\,, \tag{4.4}$$

Taking into account that at the star cluster center $u_w = 0$ and $\dfrac{du_w}{dr}$ is finite, one can obtain

$$(\gamma-1)(q_{eo}-Q_c) = \left[q_m c_s^2+\rho_w u_w\frac{dc_s^2}{dr}\right]\Bigg|_{r=0}\,, \tag{4.5}$$

where the derivative of the sound speed with respect to the distance to the star cluster center.

Substituting the derivative of the sound speed $\frac{dc_s^2}{dr}$ (obtained in Appendix B) into (4.5) and taking into account that at the star cluster center the terms $\gamma\rho_w u_w^2 \frac{du_w}{dr}$ and $\gamma u_w^2 q_m$ vanish, one can obtain

$$(\gamma-1)(q_{eo}-Q_c) \;=\; \left[\rho_w c_s^2 \frac{du_w}{dr} + \frac{2\rho_w u_w c_s^2}{r}\right]\Bigg|_{r=0} \tag{4.6}$$

Equations (3.8) and (4.3) allow to calculate the value of the last term of equation (4.6) when $r \to 0$

$$2\rho_{wo}c_c^2 \lim_{r\to 0}\frac{u_w}{r} \;=\; 2\rho_{wo}c_c^2\left[\frac{(\gamma-1)(q_{eo}-Q_c)-\frac{2}{3}q_{mo}c_c^2}{\rho_{wo}c_c^2}\right] \tag{4.7}$$

which leads to

$$2\rho_{wo}c_c^2 \lim_{r\to 0}\frac{u_w}{r} \;=\; 2(\gamma-1)(q_{eo}-Q_c) - \frac{4}{3}q_{mo}c_c^2\,. \tag{4.8}$$

and equation (4.6) turns into

$$q_{mo}c_c^2 \;=\; (\gamma-1)(q_{eo}-Q_c)\,. \tag{4.9}$$

Taking into account that $Q_c = n_{wo}^2\Lambda(T_c,Z)$, one can finally obtain

$$q_{mo}c_c^2 = (\gamma-1)[q_{eo}-n_{wo}^2\Lambda(T_c,Z)]\,, \tag{4.10}$$

Equation (4.10) shows that the wind central density n_{wo} and the central temperature are not independent as in the adiabatic case (Chevalier & Clegg, 1985; Raga et al., 2001), but are related by the equation

$$n_{wo} = \left[\frac{q_{eo}-\frac{q_{mo}c_c^2}{\gamma-1}}{\Lambda(T_c)}\right]^{1/2} = q_{mo}^{1/2}\left[\frac{\frac{u_{A\infty}^2}{2}-\frac{c_c^2}{\gamma-1}}{\Lambda(T_c)}\right]^{1/2}\,, \tag{4.11}$$

where c_c is the sound speed at the star cluster center. Equation (4.11) is consistent with the relation found by Sarazin & White (1987) from the energy conservation equation in their cooling flow model and that found by Silich et al. (2004) for star clusters with homogeneous stellar density distribution.

The term $\left[\frac{u_{A\infty}^2}{2} - \frac{c_c^2}{\gamma - 1}\right]$ in equation (4.11) cannot be negative in order to have a density with a physical meaning. This is why the central temperature T_c cannot exceed the adiabatic wind value

$$T_c^{max} = \frac{(\gamma - 1)\mu_{ion} u_{A\infty}^2}{2\gamma k_B} \, . \tag{4.12}$$

In order to start the numerical integration, one has to take a small step away, ΔR_1, from the star cluster center, and use as initial conditions

$R_w = \Delta R_1$,

$u_w = u_{wo} + \left.\frac{du_w}{dr}\right|_0 \Delta R_1$,

$\rho_w = \frac{2 q_{mo} R_c^3}{u_w R_w^2}\left[1 - \left(1 + \frac{R_w}{R_c} + \frac{1}{2}\frac{R_w^2}{R_c^2}\right) e^{-R_w/R_c}\right]$,

$P_w = P_{wo}$.

4.3 The Boundary Conditions

The boundary condition which allows to select the wind solution from the infinite number of integral curves is that the integral curve must pass through the singular point. The derivative of the expansion velocity at the singular point must be positive (Lamers & Cassinelli, 2007). At the singular point, the numerator, N, and the denominator, D, of equation (3.13) simultaneously vanish. Thus at the singular point

$$c_{sp} = u_{sp} \, . \tag{4.13}$$

where c_{sp} and u_{sp} are the values of the sound speed and the wind velocity at the singular point. In other words, in this case the singular point coincides with the sonic point.

Substitution of (4.13) into (3.13) yields

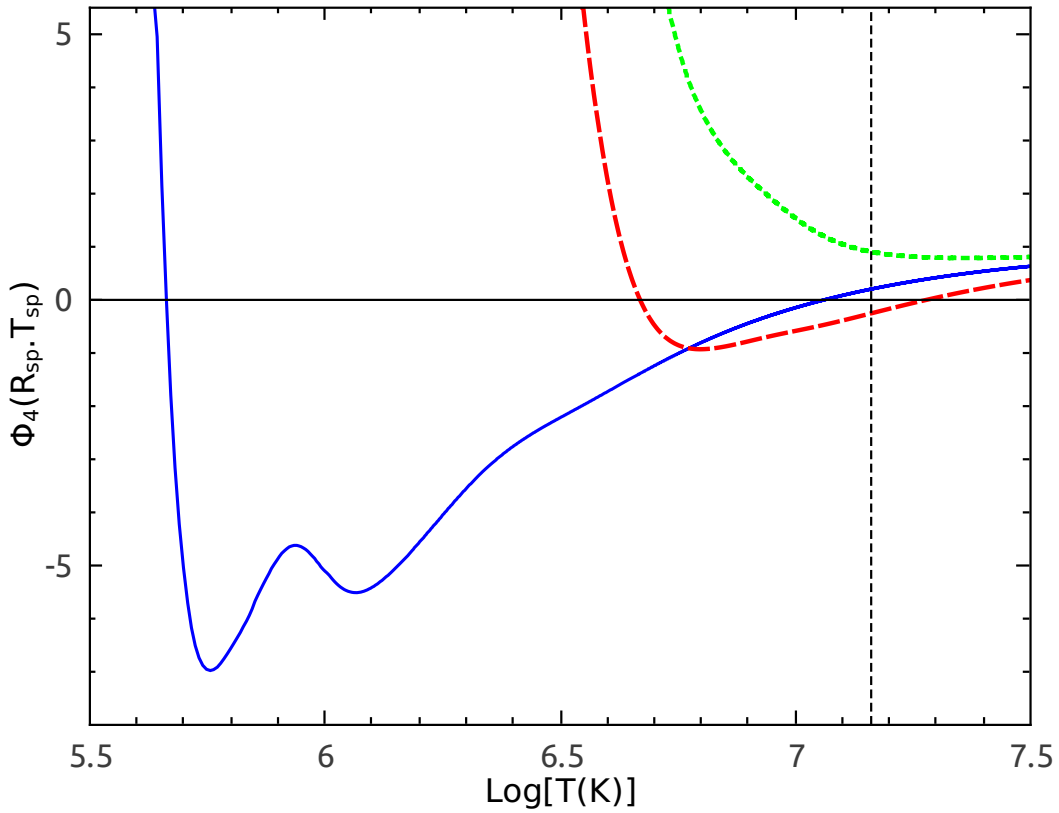

Figure 4.2: Function $\Phi_4(R_{sp}, T_{sp})$ for different mechanical luminosities and trial singular radii. The solid line corresponds to the model for $L_{sc} = 3 \times 10^{40}$ erg s^{-1} and $R_{sp} = 4$ pc. The large-dashed line displays the model for $L_{sc} = 7 \times 10^{41}$ erg s^{-1} and $R_{sp} = 3.4$ pc. The short-dashed line presents the model for $L_{sc} = 3 \times 10^{42}$ erg s^{-1} and $R_{sp} = 3$ pc. Thin vertical dashed line marks the adiabatic wind central temperature. In all cases the star cluster core radius was taken as 1 pc and the adiabatic wind terminal velocity as $u_{A\infty} = 1000$km s^{-1}.

$$(\gamma - 1)(q_e - Q) - \frac{4q_{mo}c_s^2 R_c^3}{R_{sp}^3}(1 - e^{-R_{sp}/Rc}) + q_m \left[\frac{c_s^2(\gamma + 1)}{2} + \frac{4c_s^2 R_c^3}{R_{sp}^3}\left(\frac{R_{sp}}{R_c} + \frac{1}{2}\frac{R_{sp}^2}{R_c^2}\right)\right] = 0. \tag{4.14}$$

Equation (4.14) leads to a quadratic equation for the sound speed at the singular point

$$c_s^2 = g_1 \pm \sqrt{g_1^2 - g_2 \Lambda(T_{sp}, Z)}\,, \tag{4.15}$$

where g_1, g_2 and g_3 are functions of R_{sp}

$$g_1 = \frac{\gamma - 1}{4g_3} u_{A\infty}^2 e^{-R_{sp}/R_c} \,, \tag{4.16}$$

$$g_2 = \frac{4(\gamma-1) q_{mo} R_c^6}{g_3 \mu_{ion}^2 R_{sp}^4} \left[1 - \left(1 + \frac{R_{sp}}{R_c} + \frac{1}{2} \frac{R_{sp}^2}{R_c^2} \right) e^{-R_{sp}/R_c} \right]^2 \,, \tag{4.17}$$

and

$$g_3 = 4 \left(\frac{R_c}{R_{sp}} \right)^3 \left(1 - e^{-R_{sp}/R_c} \right) - \left[\frac{(\gamma+1)}{2} + 4 \left(\frac{R_c}{R_{sp}} \right)^2 + \frac{2R_c}{R_{sp}} \right] e^{-R_{sp}/R_c}. \tag{4.18}$$

Equation (4.15) is a non-linear algebraic equation and it must be solved numerically. It can be rewritten as

$$\Phi_4(R_{sp}, T_{sp}) = c_s^4 - 2 g_1 c_s^2 + g_2 \Lambda(T_{sp}, Z) = 0 \,, \tag{4.19}$$

I solved equation (4.19) using a bisection scheme.

Figure 4.2 displays function $\Phi_4(R_{sp}, T_{sp})$ for different values of L_{sc} in the case when $u_{A\infty} = 1000$ km s^{-1} and $R_c = 1$ pc. This figure also shows that the function $\Phi_4(R_{sp}, T_{sp})$ may have one or two real roots below T_c^{max} or no real roots.

Thus, one can obtain the temperature at the singular point using equation (4.19) if R_{sp} is known. Figure 4.3 presents the temperature at the singular point for a range of trial radii. the proper integral curve is obtained from the outward integration from the star cluster center and the inward integration from the singular point, then the two integrations must match at an intermediate radius. Usually, the root of equation (4.19) that allows to match the integral curves is the one that is closer to T_c^{max}. However, if the energy is very high or the star cluster is very compact, the value of this temperature exceeds T_c^{max} and the other root must be used to obtain the characteristic temperature of the wind at the singular point. This will be discussed in more detail in Chapter 5.

The derivative of the wind velocity at the singular point must be obtained applying the L'Hôpital's Rule

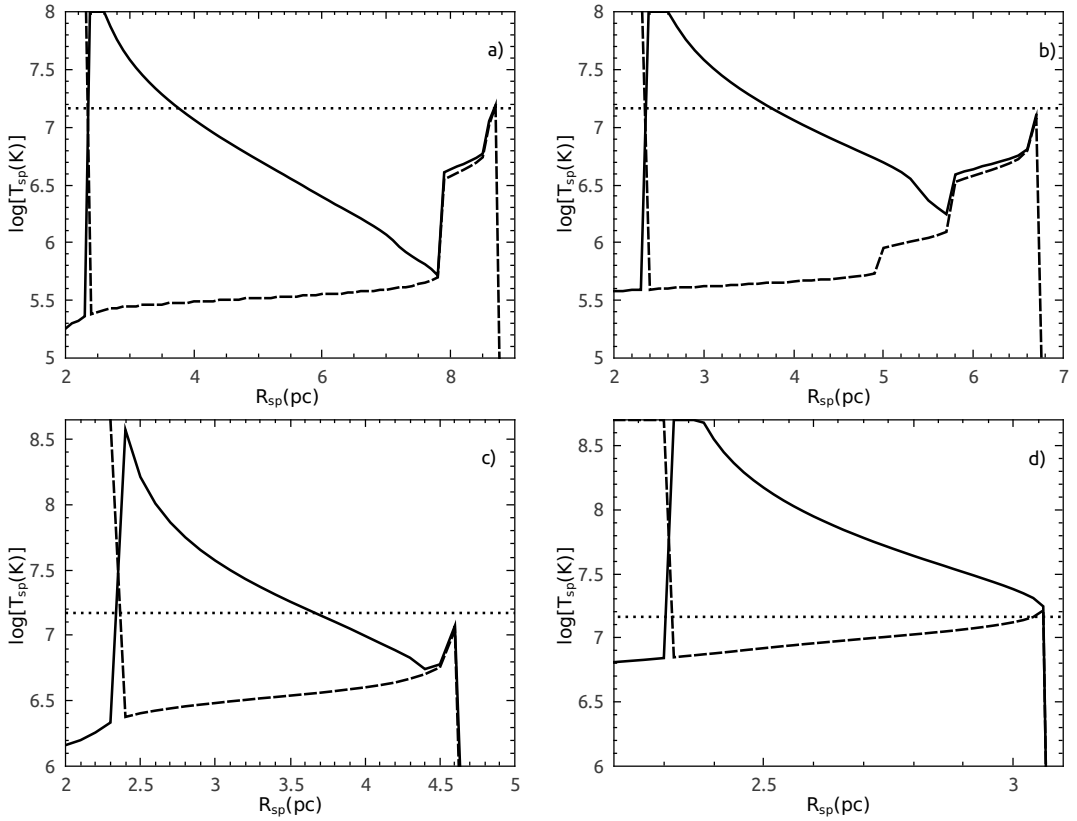

Figure 4.3: The temperature at the singular point *versus* the trial singular radius. The terminal velocity of the star cluster wind is assumed to be 1000 km s^{-1} and the star cluster core radius $R_c = 1pc$. The solid line corresponds to the root that is closer to T_c^{max} in equation (4.19) and the dashed line corresponds to the other root. Panel a) corresponds to $M_{sc} = 10^5 \mathrm{M}_\odot$, Panel b) to $M_{sc} = 10^6 \mathrm{M}_\odot$, Panel c) to $M_{sc} = 10^7 \mathrm{M}_\odot$ and Panel d) to $M_{sc} = 10^8 \mathrm{M}_\odot$.

$$\lim_{r\to R_{sp}} \frac{du_w}{dr} = \lim_{r\to R_{sp}} \frac{\dfrac{\partial N}{\partial Q}\dfrac{dQ}{dr} + \dfrac{\partial N}{\partial c_s^2}\dfrac{dc_s^2}{dr} + \dfrac{\partial N}{\partial u_w}\dfrac{du_w}{dr} + \dfrac{\partial N}{\partial r}}{\dfrac{\partial D}{\partial c_s^2}\dfrac{dc_s^2}{dr} + \dfrac{\partial D}{\partial u_w}\dfrac{du_w}{dr}} \,. \tag{4.20}$$

Here the derivatives are

$$\frac{\partial N}{\partial Q}\frac{dQ}{dr} = -(\gamma - 1)\left[\frac{2Q}{\rho_w}\frac{d\rho_w}{dr} + \frac{Q}{\Lambda}\frac{T_{sp}}{c_s^2}\frac{\mu_{tot}}{\mu_{ion}}\frac{d\Lambda}{dT}\frac{dc_s^2}{dr}\right] , \tag{4.21}$$

$$\frac{\partial N}{\partial c_s}\frac{dc_s}{dr} = \left[-\frac{4q_{mo}R_c^3}{R_{sp}^3}(1 - e^{-R_{sp}/R_{sc}}) + 4q_m\frac{R_c^3}{R_{sp}^3}\left(\frac{R_{sp}}{R_c} + \frac{1}{2}\frac{R_{sp}^2}{R_c^2}\right)\right]\frac{dc_s^2}{dr} , \tag{4.22}$$

$$\frac{\partial N}{\partial u_w}\frac{du_w}{dr} = (\gamma+1)c_s q_m \,, \tag{4.23}$$

$$\begin{aligned}\frac{\partial N}{\partial r} &= (1-\gamma)\frac{q_e}{R_c} - \frac{1}{2}(\gamma+1)q_m\frac{c_s^2}{R_c} + \frac{12 q_{mo} R_c^3 c_s^2}{R_{sp}^4}(1-e^{-R_{sp}/R_c}) \\ &- \frac{12 q_m R_c^2 c_s^2}{R_{sp}^3} - \frac{6 q_m R_c c_s^2}{R_{sp}^2} - \frac{2 q_m c_s^2}{R_{sp}} \,,\end{aligned} \tag{4.24}$$

and

$$\frac{dD}{dr} = \frac{\partial D}{\partial c_s^2}\frac{dc_s^2}{dr} + \frac{\partial D}{\partial u_w}\frac{du_w}{dr} = \frac{dc_s^2}{dr} - 2c_s\frac{du_w}{dr} \,. \tag{4.25}$$

The derivatives of the wind density and the local sound speed (cf. Appendices A and B) at the singular point are

$$\frac{d\rho_w}{dr} = -\frac{du_w}{dr}\frac{\rho_w}{c_s} + \frac{q_m}{c_s} - \frac{2\rho_w}{R_{sp}} \,, \tag{4.26}$$

and

$$\frac{dc_s^2}{dr} = -\frac{du_w}{dr}(\gamma-1)c_s - \frac{(\gamma+1)c_s q_m}{\rho_w} + \frac{2c_s^2}{R_{sp}} \,, \tag{4.27}$$

respectively.

Equation (4.20) leads to a quadratic equation for the derivative of the wind velocity at the singular point

$$\begin{aligned}&- (\gamma+1)c_s\rho_w\left(\frac{du_w}{dr}\right)^2 + \left[\frac{2c_s^2\rho_w}{R_{sp}} - (\gamma+1)c_s q_m\right]\frac{du_w}{dr} = f_1 + f_2\left[-\frac{(\gamma+1)c_s q_m}{\rho_w} + \frac{2c_s^2}{R_{sp}}\right] \\ &+ \frac{du_w}{dr}\left[\frac{2Q(\gamma-1)}{c_s} + \frac{Q(\gamma-1)^2}{\Lambda}\frac{T_{sp}}{c_s^2}\frac{\mu_{tot}}{\mu_{ion}}\frac{d\Lambda}{dT} + (\gamma+1)c_s q_m - (\gamma-1)f_2 c_s\right] + \frac{\partial N}{\partial r} \,,\end{aligned} \tag{4.28}$$

where functions f_1 and f_2 are

$$f_1 = -(\gamma - 1)\left\{\frac{2Qq_m}{\rho_w c_s} - \frac{4Q}{R_{sp}} - \frac{Q}{\Lambda}\frac{(\gamma+1)q_m T_{sp}}{c_s \rho_w}\frac{\mu_{tot}}{\mu_{ion}}\frac{d\Lambda}{dT} + \frac{2QT_{sp}}{\Lambda R_{sp}}\frac{d\Lambda}{dT}\right\}\ , \quad (4.29)$$

$$f_2 = -\frac{4q_{mo}R_c^3}{R_{sp}^3}(1 - e^{-R_{sp}/R_{sc}}) + 4q_m\frac{R_c^3}{R_{sp}^3}\left(\frac{R_{sp}}{R_c} + \frac{1}{2}\frac{R_{sp}^2}{R_c^2}\right)\ . \quad (4.30)$$

Equation (4.28) has two solutions. One has to select the solution which results into positive derivative of the wind velocity at the singular point

$$\frac{du_w}{dr} = \frac{a_1 + \sqrt{a_1^2 + 4a_o a_2}}{2a_2}\ , \quad (4.31)$$

where a_0, a_1 and a_2 are

$$a_0 = -\left[f_1 + f_2\left[-\frac{(\gamma+1)c_s q_m}{\rho_w} + \frac{2c_s^2}{R_{sp}}\right] + \frac{\partial N}{\partial r}\right]\ ,$$

$$a_1 = \frac{2c_s^2\rho_w}{R_{sp}} - 2(\gamma+1)c_s q_m - \frac{2Q(\gamma-1)}{c_s} - \frac{Q(\gamma-1)^2}{\Lambda}\frac{T_{sp}}{c_s^2}\frac{\mu_{tot}}{\mu_{ion}}\frac{d\Lambda}{dT} + f_2(\gamma-1)c_s\ ,$$

and

$$a_2 = -(\gamma+1)c_s\rho_w\ .$$

The determination of the wind velocity gradient at the singular point allows one to determine the analytic boundary conditions required to integrate the hydrodynamic equations. It also allows a smooth transition through a region where the numerical calculation is unstable as it may vary between large positive and negative values in a short distance interval (Lamers & Cassinelli, 2007).

Figure 4.4 shows the derivative of the wind velocity at the singular point for the case when $M_{sc} = 10^6 M_\odot$, $u_{A\infty} = 1000$ km s^{-1} and $R_c = 1$ pc.

In order to start the numerical integration, one has to take a small step away, ΔR_2, using the following analytic expansions

$$R_w = R_{sp} + \Delta R_2\ ,$$

$$u_w = c_{sp} + \left.\frac{du_w}{dr}\right|_{R_{sp}} \Delta R_2\ ,$$

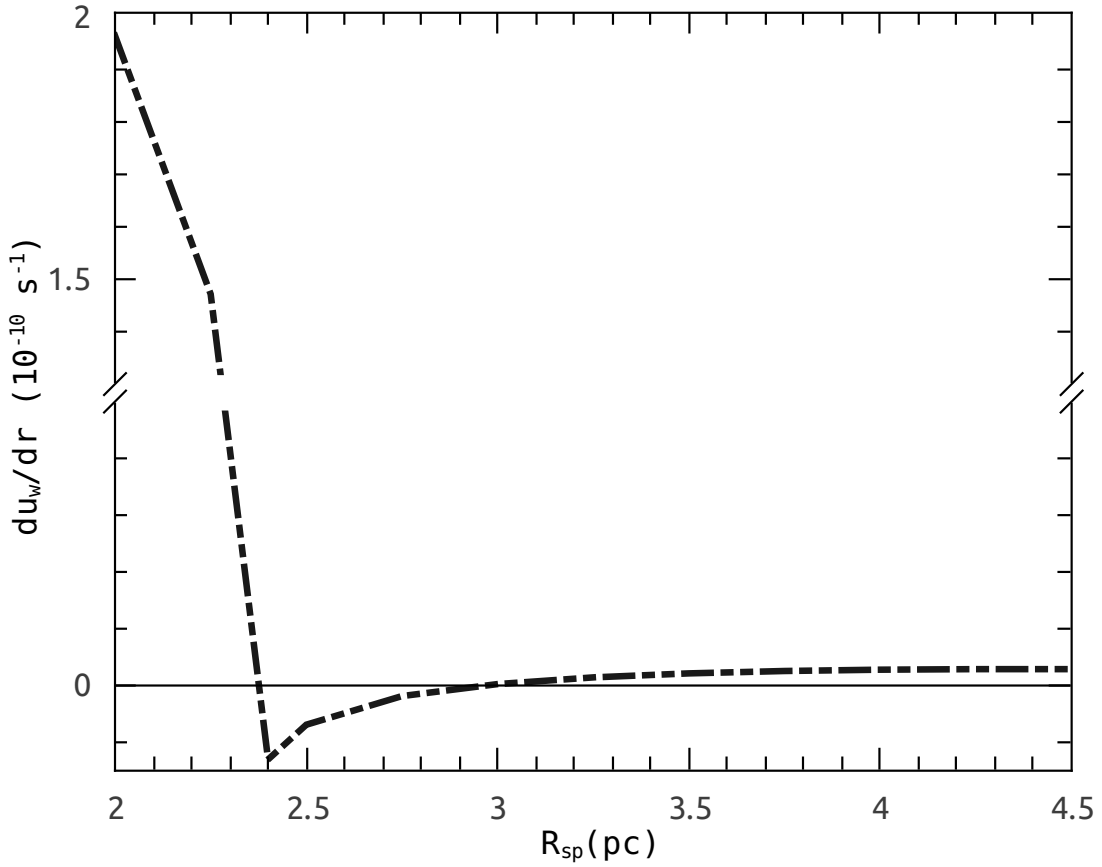

Figure 4.4: The derivative of the wind velocity for different trial special point radii. The total mass of the star cluster is assumed to be $M_{sc} = 10^6 \mathrm{M}_\odot$, terminal velocity 1000 km s^{-1} and the star cluster core radius $R_c = 1$ pc. This curve constrains the range of possible singular point radii because only positive values of the derivative of the wind velocity are allowed for a wind.

$$\rho_w = \frac{2q_{mo}R_c^3}{u_w R_w^2}\left[1 - \left(1 + \frac{R_w}{R_c} + \frac{1}{2}\frac{R_w^2}{R_c^2}\right)e^{-R_w/R_c}\right] ,$$

$$\frac{dP_w}{dr} = -\rho_w c_{sp}\left.\frac{du_w}{dr}\right|_{R_{sp}} - q_m c_{sp} ,$$

$$P_w = P_{sp} + \left.\frac{dP_w}{dr}\right|_{R_{sp}} \Delta R_2 .$$

The code employed for solving equations (3.10) and (3.13) uses the well-known integrator called Stiff which applies the Adams' Method. At each step of the integration, Stiff automatically selects the step size of the integration according to the required accuracy.

Chapter 5

Results from the Calculations

In this chapter, I present the results from the calculations for winds driven by SSCs with an exponential stellar density distribution for a variety of input parameters using the semi-analytic method described in the preceding chapter. For this purpose, I first compare the runs of velocity and temperature obtained from semi-analytic radiative calculations to the non-radiative numeric results from Ji et al. (2006). Then I define a *reference model*, which represents a typical SSC. The distribution of the flow variables (velocity, temperature, particle number density, thermal pressure and ram pressure) obtained for the *reference model* are then compared to those calculated in models with other input parameters.

5.1 Comparison with previous results

Ji et al. (2006, hereafter JWK06) have considered numerically the case of super star clusters with an exponential stellar density distribution. However, in their hydrodynamic calculations they did not take into account the effects of radiative cooling. They used the following input parameters: a star cluster core radius $R_c = 0.48$ pc, a mass deposition rate $\dot{M}_{sc} = 10^{-4}\,\mathrm{M}_{\odot}\,yr^{-1}$ and three adiabatic wind terminal velocities $u_{A\infty} = 500$, 1000 and 2000 km s^{-1} (from now on, JWK500, JWK1000 and JWK2000 cases, respectively).

In order to verify the semi-analytic method presented here, I carried out calculations for the same input parameters. I used L_{sc} instead of $\dot{M}_{sc}$ as an input parameter using

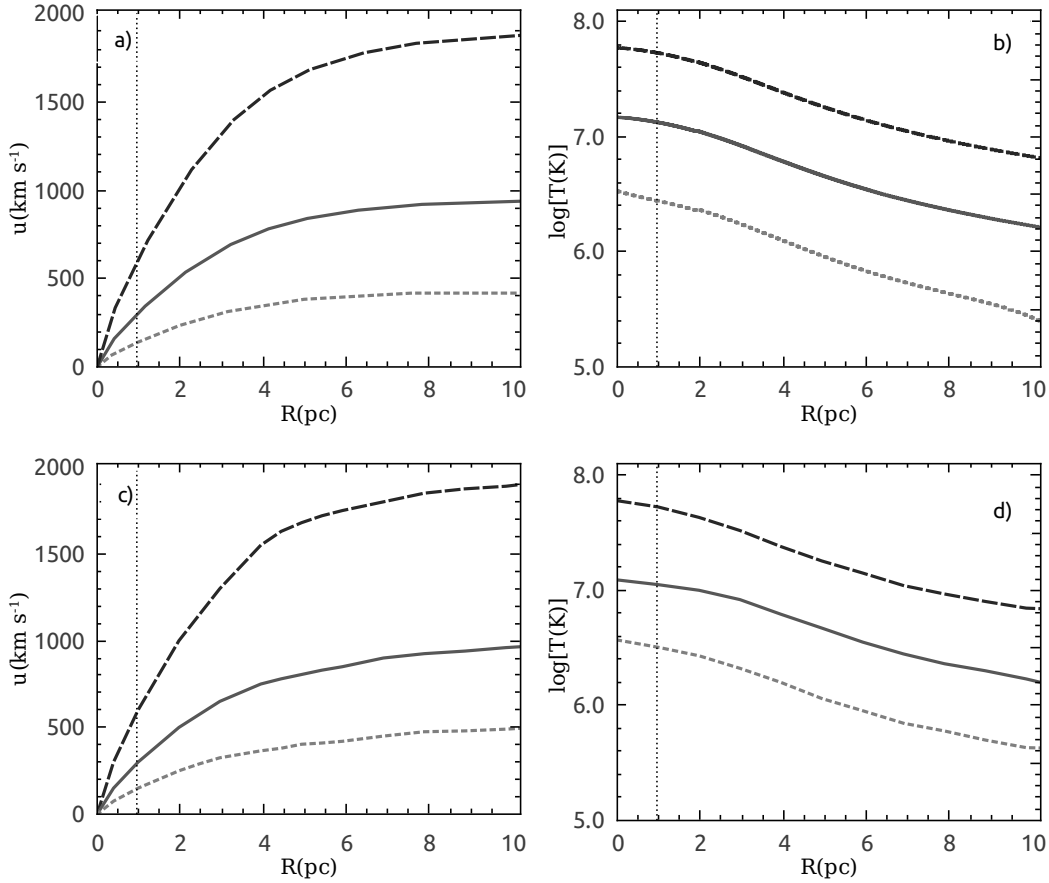

Figure 5.1: The comparison of the semi-analytical radiative calculation to the numeric results of Ji et al. (2006). Short-dashed, solid and long-dashed lines present the results of the calculations for JWK500, JWK1000 and JWK2000, respectively. Panels a) and b) depict the runs of velocity and temperature obtained with the semi-analytic method. The vertical line marks the location of the singular point. I adapted panels c) and d) to show the results of the JWK06.

the relation $L_{sc} = \frac{1}{2}\dot{M}_{sc}u^2_{A\infty}$. Figure 5.1 displays the results of these calculations (top panels) and compare them to the results obtained by JWK06 (bottom panels). The two methods are in excellent agreement. JWK obtained that the singular point is located at $R_{sp} = 1.97$ pc. In the semi-analytic radiative wind calculations, the singular point is located at $R_{sp} = 1.93$ pc, $R_{sp} = 1.93$ pc and $R_{sp} = 1.94$ pc, for the JWK500, JWK1000 and JWK2000 cases, respectively.

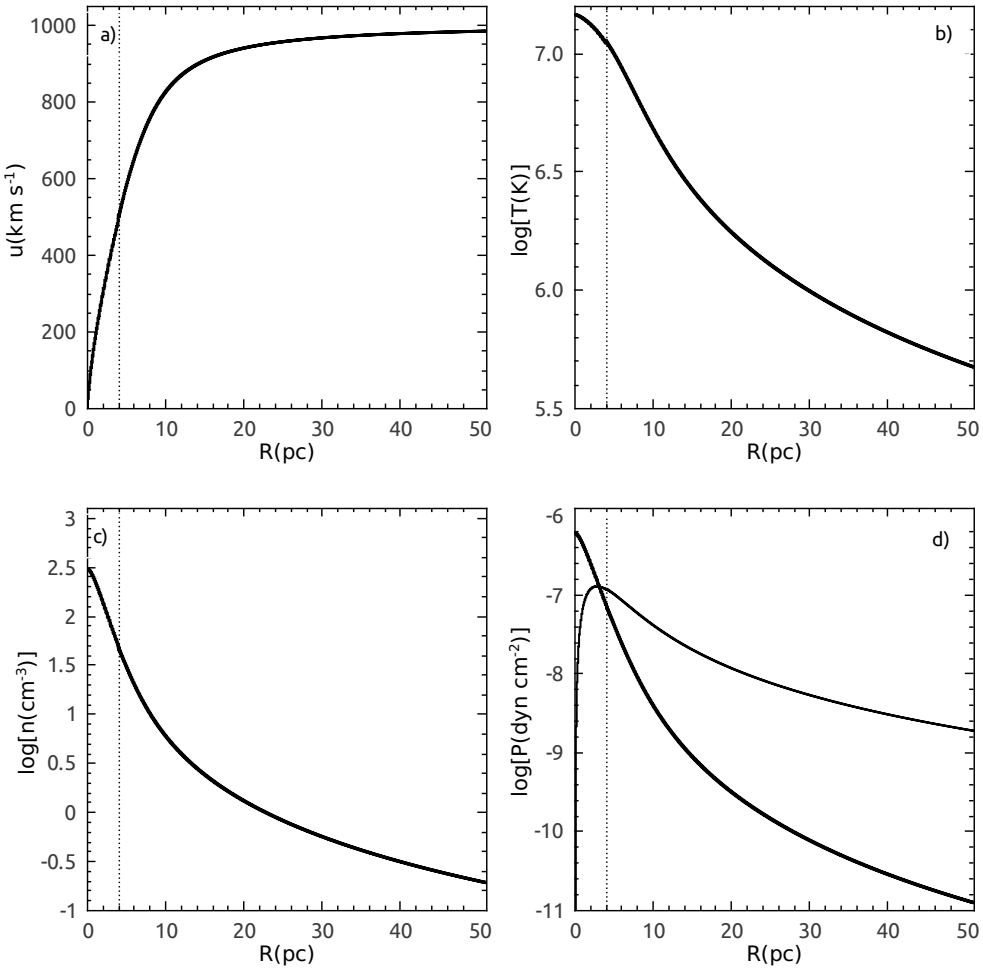

Figure 5.2: The reference model. Panels a), b) and c) show the runs of the flow variables for model A. Thick and thin lines in panel d) present the runs of thermal and ram pressure, respectively. The vertical line marks the location of the singular point.

5.2 The Reference Model

The *reference model* (hereafter model A) has the following input parameters: a total stellar mass equal to $10^6 M_\odot$ which leads to an average mechanical luminosity $L_{sc} = 3 \times 10^{40}$ erg s^{-1}. I have selected an adiabatic wind terminal velocity $u_{A\infty} = 1000$ km s^{-1}, a star cluster core radius $R_c = 1$ pc and solar metallicity $Z = Z_\odot$.

The runs of the flow variables for the *reference model* are shown in Figure 5.2. The expansion velocity of the outflow in the *reference model* A grows from $u_w = 0$ km s^{-1} at the star cluster center to reach the local sound speed ($u_{sp} = c_{sp} = 500$ km s^{-1}) at

the singular point at $R_{sp} = 4.04$ pc (cf. Panel *a)*). It continues then to grow rapidly and reaches the terminal value $v_\infty \sim 990$ km s^{-1}. This velocity is slightly smaller than the adiabatic wind terminal velocity $u_{A\infty}$. These two values would only coincide in the absence of radiative cooling, because some fraction of the energy deposited in the flow is radiated away.

The wind temperature decreases rapidly from its central value $T_c \sim 1.46 \times 10^7$ K to $T_{sp} \sim 1.1 \times 10^7$ K at the singular point (cf. Panel *b)*). The particle number density and the thermal pressure have rapid decays from their central values (cf. Panels *c)* and *d)*). The ram pressure, $P_{RAM} = \rho_w u_w^2$, and the thermal pressure are equal at a radius $R_{RAM} \sim 3$ pc.

5.3 The Quasi-Adiabatic Regime

In this section, I compare the results obtained in the prior section to models with different mechanical luminosities, star cluster core radii and adiabatic wind terminal velocities. The input parameters of each model are presented in Table 5.1.

Model	L_{sc}(erg s^{-1})	R_c(pc)	$u_{A\infty}$(km s^{-1})	$Z(Z_\odot)$
A	3×10^{40}	1.0	1000	1.0
B	3×10^{39}	1.0	1000	1.0
C	3×10^{41}	1.0	1000	1.0
D	3×10^{40}	0.2	1000	1.0
E	3×10^{40}	5.0	1000	1.0
F	3×10^{40}	1.0	750	1.0
G	3×10^{40}	1.0	2000	1.0

Table 5.1: Input parameters for models A, B, C, D, E, F and G.

In all these models, the outflow is quasi-adiabatic. This implies that the energy carried away from the star cluster is small compared to the energy supplied by massive stars and radiative cooling affects the flow at large or very large radii and therefore does not affect the location of the singular point.

The runs of the flow variables for models A, B and C are shown in Figure 5.3. In the case of model B, the outflow velocity u_w equals the local sound speed, $u_{sp} = 501.8$ km s^{-1}, at $R_{sp} = 4.04$ pc (cf. Panel *a)*). The wind temperature decreases from

the central value $T_c \sim 1.4 \times 10^7$ K to $T_{sp} \sim 1.1 \times 10^7$ K at the singular point (cf. Panel *b)*). The density of the wind in model B is lower than in model A, by about one order of magnitude (cf. Panel *c)*). Indeed, combining equations (2.2), (3.4) and (3.8), one can obtain

$$\rho_w = \frac{L_{sc}}{2\pi u_w u_{A\infty}^2 r^2} \left[1 - \left(1 + \frac{r}{R_c} + \frac{1}{2}\frac{r^2}{R_c^2} \right) e^{-r/R_c} \right] , \tag{5.1}$$

Equation (5.1) shows that the wind density must grow when L_{sc} increases and decrease with increasing $u_{A\infty}$ and R_c.

In model C, the density is approximately one order of magnitude higher than in model A (cf. Panel *c)*). The singular point is located at $R_{sp} = 4.02$ pc, where the wind velocity is $u_{sp} = 466.1$ km s^{-1} (cf. Panel *a)*). In this case, the wind temperature decreases from the central value $T_c \sim 1.3 \times 10^7$ K to $T_{sp} \sim 9.6 \times 10^6$ K at the singular point. Note that the wind temperature begins to depart from the quasi-adiabatic regime at approximately ~ 10 pc from the star cluster center in model C. The impact of radiative cooling becomes more noticeable at about ~ 35 pc where the wind temperature drops rapidly to the lowest permitted value $T_w = 10^4$ K value (cf. Panel *b)*). This leads to a fast decrease of the thermal pressure at the same distance (cf. Panel *d)*).

The distribution of the flow variables for models with different core radii (models D and E) are shown in Figure 5.4. The singular point in model D is located at $R_{sp} = 0.8$ pc, where the expansion velocity is $u_{sp} = 486$ km s^{-1} (cf. Panel *a)*). The particle number density at the star cluster center in model D is one order of magnitude higher than in model A. However, it experiences a rapid decay and at larger radii approaches the resultant density of model A (cf. Panel *c)*). The wind temperature T_w rapidly decreases from $T_c \sim 1.4 \times 10^7$ K at the star cluster center to $T_{sp} \sim 1.0 \times 10^7$ K at the singular point. Then the temperature profile begins to deviate from the quasi-adiabatic profile at a distance of ~ 10 pc because of strong radiative cooling (cf. Panel *b)*). This promotes a strong decay in the thermal pressure at the same distance (cf. Panel *d)*).

In model E, the singular point is located at $R_{sp} = 20.2$ pc, where the wind velocity is $u_{sp} = 501$ km s^{-1} (cf. Panel *a)*). In this case, the wind temperature decreases from $T_c \sim 1.4 \times 10^7$ K at the star cluster center to $T_{sp} \sim 1.1 \times 10^6$ K at the singular point (cf. Panel *b)*). The particle number density in this model decreases slowly than in model D and becomes comparable to the wind density for model A at about ~ 10 pc (cf. Panel

c)).

The runs of the flow variables for models with different adiabatic wind terminal velocities (models F and G) are shown in Figure 5.5. In model F, the singular point is at $R_{sp} = 4.03$ pc, where the wind velocity is $u_{sp} = 361.3$ km s^{-1} (cf. Panel *a)*). The wind temperature decreases from $T_c \sim 7.81 \times 10^6$ K at the star cluster center to $T_{sp} \sim 5.81 \times 10^6$ K at the singular point. The temperature and thermal pressure drop fast at a distance ~ 32 pc (cf. Panels *b)* and *d)*). The wind density in this model is half an order of magnitude higher than in model A (cf. Panel *c)*).

The singular point in model G occurs at $R_{sp} = 4.04$ pc, where the outflow velocity is $u_{sp} = 1005$ km s^{-1} (cf. Panel *a)*). The wind temperature is much larger than in other models. It is $T_c \sim 5.9 \times 10^7$ K at the star cluster center and drops to $T_{sp} \sim 4.46 \times 10^7$ K at the singular point (cf. Panel *b)*). In this case, the particle number density is lower than in model A by an order of magnitude (cf. Panel *c)*).

Note that in all quasi-adiabatic models, the singular point is located at a distance $R_{sp} \approx 4R_c$. The outflow velocity at the singular point is $u_{sp} \approx \frac{1}{2}u_{A\infty}$, which is also the case for star clusters with a homogeneous stellar density distribution (Chevalier & Clegg, 1985). The ram pressure, P_{RAM}, equals the thermal pressure, P_w, at a radius, $R_{_{RAM}}$, about three times larger than the star cluster core radius R_c. There is also an approximate relation between the wind central temperature and the singular point temperature $T_{sp} \approx \frac{3}{4}T_c$. All these approximate relations are almost insensitive to changes in the input parameters: adiabatic wind terminal velocity, star cluster core radius and mechanical luminosity (cf. Appendix C). Moreover, changes in the gas metallicity, do not change these approximate relations as long as the metallicity is small enough to preserve the wind in the quasi-adiabatic regime.

5.4 The Catastrophic Cooling Regime

Winds driven by SSCs with high mechanical luminosities, small star cluster core radii, low adiabatic wind terminal velocities or high metallicities are strongly affected by radiative cooling. In these cases a rapid decay in temperature occurs just outside the singular point. The rapid decays in temperature are provoked by the negative slope near the maximum value of the cooling function shown in Figure 3.1.

In this regime, the singular point moves rapidly towards the star cluster center as one considers more massive clusters, smaller star cluster core radii and lower adiabatic wind terminal velocities. The flow outside of the singular point may be thermally unstable. However, to prove it, it is required to provide 1D or 2D numerical calculations which is beyond the scope of my thesis.

In order to illustrate this regime, I run a model, hereafter model H, with the following input parameters: an average mechanical luminosity $L_{sc} = 7 \times 10^{41}$ erg s^{-1}, an adiabatic wind terminal velocity $u_{A\infty} = 1000$ km s^{-1}, a star cluster core radius $R_c = 1$ pc and solar metallicity, $Z = \mathrm{Z}_{\odot}$.

I assumed that the flow is completely ionized at large distances from the star cluster center and the wind is isothermal when the gas cools down to 10^4 K. This is a realistic assumption, because the temperature of the gas can be maintained at 10^4 K as long as the photoionizing flux from the massive stars persists (Tenorio-Tagle et al., 2005).

The hydrodynamic equations in the case of an isothermal wind driven by star clusters with an exponential stellar density distribution are (cf. Appendix D)

$$\rho_w = \frac{2 q_{mo} R_c^3}{u_w r^2} \left[1 - \left(1 + \frac{r}{R_c} + \frac{1}{2} \frac{r^2}{R_c^2} \right) e^{-r/R_c} \right] , \tag{5.2}$$

and

$$\frac{du_w}{dr} = \frac{-\dfrac{q_m c_s^2}{\gamma u_w} + \dfrac{2\rho_w c_s^2}{\gamma r} - q_m u_w}{\rho_w \left(u_w - \dfrac{c_s^2}{\gamma u_w} \right)} . \tag{5.3}$$

Figure 5.6 shows the runs of the flow variables for model H. The wind velocity grows from $u_w = 0$ km s^{-1} at the star cluster center to its maximum value at ~ 5.5 pc (cf. Panel *a)*) where the velocity gradient becomes negative due to the rapid fall of temperature which also causes a strong decay in the thermal pressure (cf. Panels *b)* and *d)*). Then, at approximately ~ 9 pc, the wind velocity reaches $u_w \sim 400$ km s^{-1} and becomes almost a constant for larger radii.

The singular point for model H is located at $R_{sp} = 3.44$ pc, where the flow velocity is $u_{sp} = 327.4$ km s^{-1}. The wind has a central temperature of $T_c \sim 1.2 \times 10^7$ K and

goes to $T_{sp} \sim 4.7 \times 10^6$ K at the singular point radius. The temperature then rapidly falls to 10^4 K at ~ 8 pc (cf. Panel *b)*). For larger radii I used the isothermal wind approximation in order to complete the flow profiles. The wind density in this model is one and a half orders of magnitude higher than in model A.

As it has been already discussed in Chapter 4, equation (4.19), which defines the temperature at the singular point, may have two different solutions. In model H there is only one solution which leads to the temperature at the singular point, $T_{sp} < T_c^{max} = \frac{(\gamma-1)\mu_{ion}u_{A\infty}^2}{2\gamma k_B}$, where T_c^{max} is the adiabatic wind central temperature (cf. Figure 5.7). Thus in this case one cannot use the solution of equation (4.19) with the higher temperature as in the quasi-adiabatic wind models. I assume that the catastrophic cooling regime sets in when the solution with the higher temperature of equation (4.19) surpasses the value T_c^{max}.

Note that in the strong radiative regime, the position of the singular point is different from the quasi-adiabatic value.

Finally, in this case none of the approximate relations found for the quasi-adiabatic wind regime hold and the size of the X-ray envelope is drastically diminished to less than ~ 5 pc in contrast to the size that one would expect in the quasi-adiabatic cases.

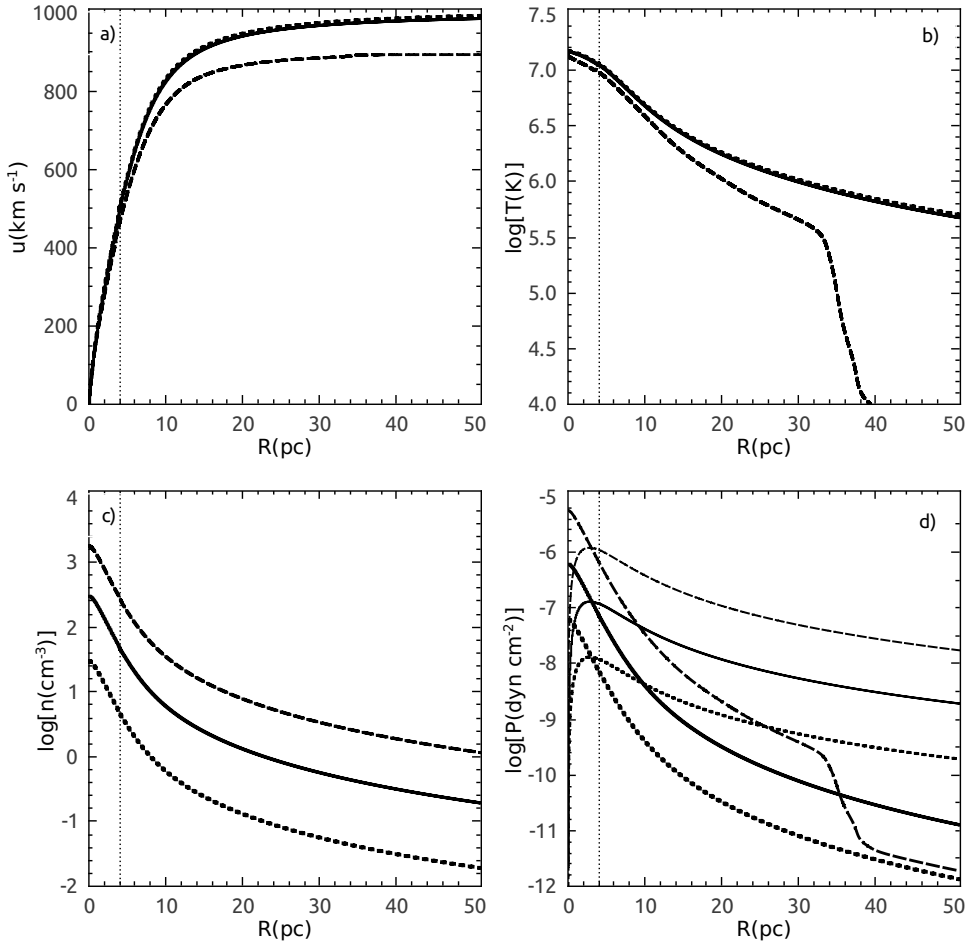

Figure 5.3: Models with different mechanical energy input rates. Panels a), b) and c) depict the runs of velocity, temperature and particle number density, respectively. Solid, Short-dashed and long-dashed lines present the results of the calculations for the models A, B and C, respectively. Thick and thin lines in panel d) present the runs of thermal and ram pressure, respectively. The vertical line marks the location of the singular point.

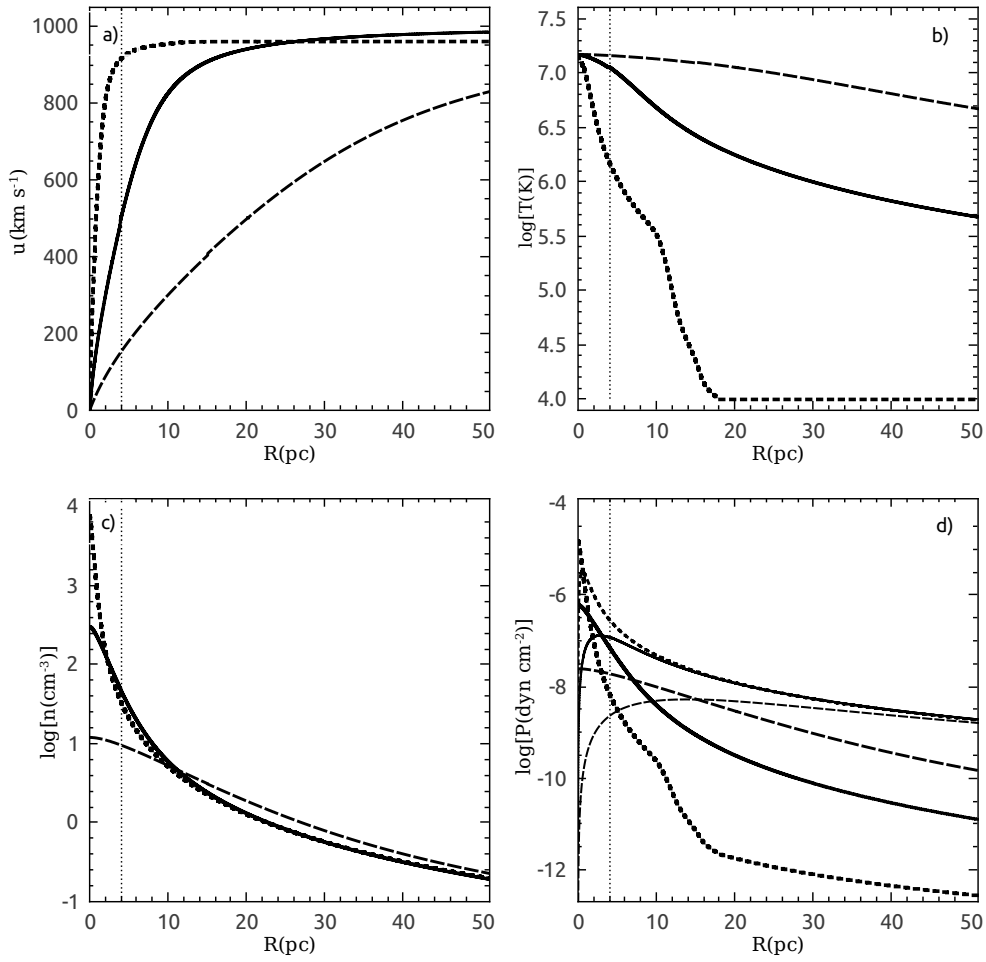

Figure 5.4: Models with different star cluster core radius. Panels a), b) and c) show the runs of velocity, temperature and particle number density, respectively. Solid, Short-dashed and long-dashed lines present the results of the calculations for the models A, D and E, respectively. Thick and thin lines in panel d) present the runs of thermal and ram pressure, respectively. The vertical line marks the location of the singular point.

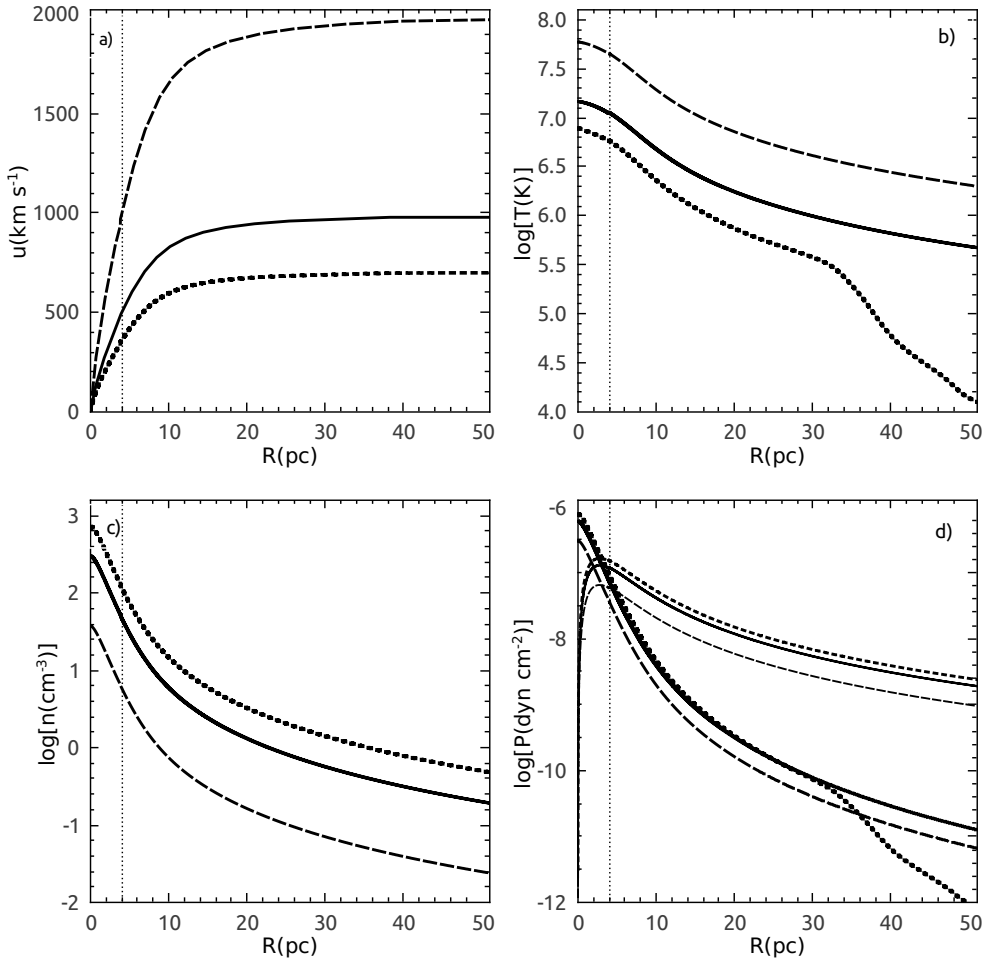

Figure 5.5: Models with different adiabatic wind terminal velocity. Panels a), b) and c) display the runs of velocity, temperature and particle number density, respectively. Solid, Short-dashed and long-dashed lines present the results of the calculations for the models A, F and G, respectively. Thick and thin lines in panel d) present the runs of thermal and ram pressure, respectively. The vertical line marks the location of the singular point.

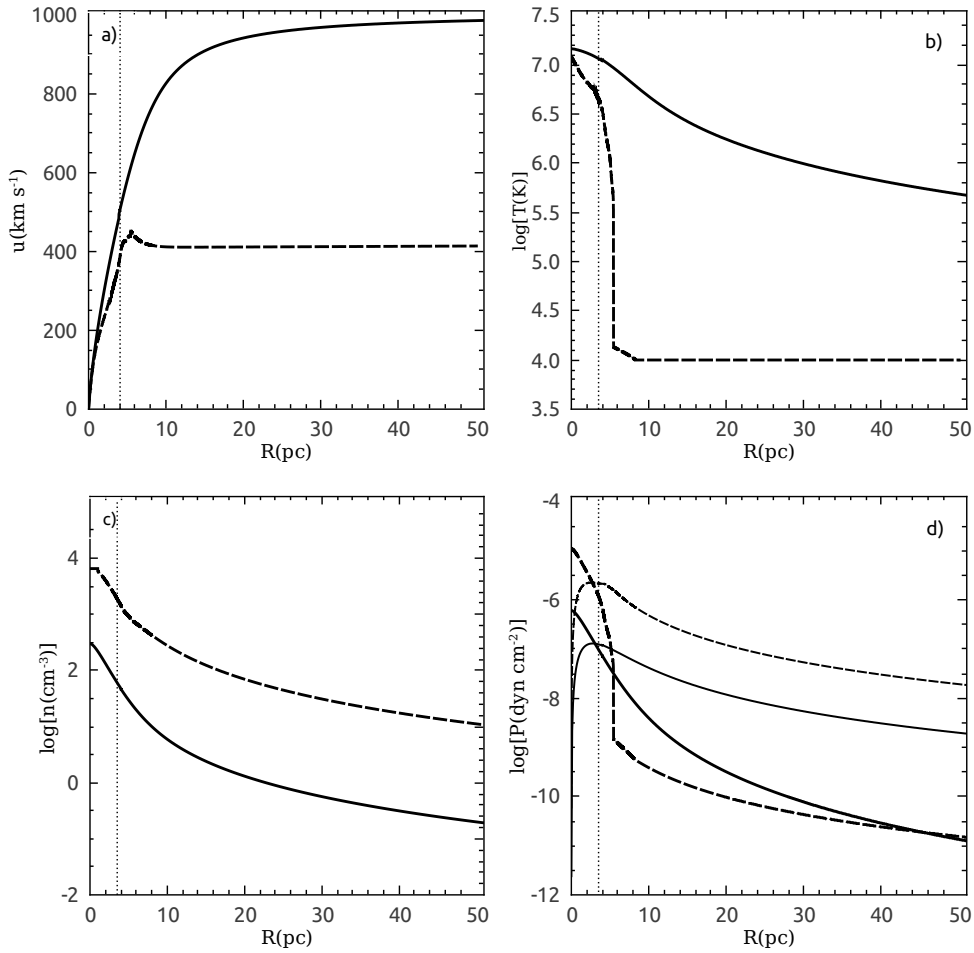

Figure 5.6: The catastrophic cooling regime. Panels a), b) and c) display the runs of velocity, temperature and particle number density, respectively. Solid and long-dashed lines present the results of the calculations for the models A and H, respectively. Thick and thin lines in panel d) present the runs of thermal and ram pressure, respectively. The vertical line marks the location of the singular point.

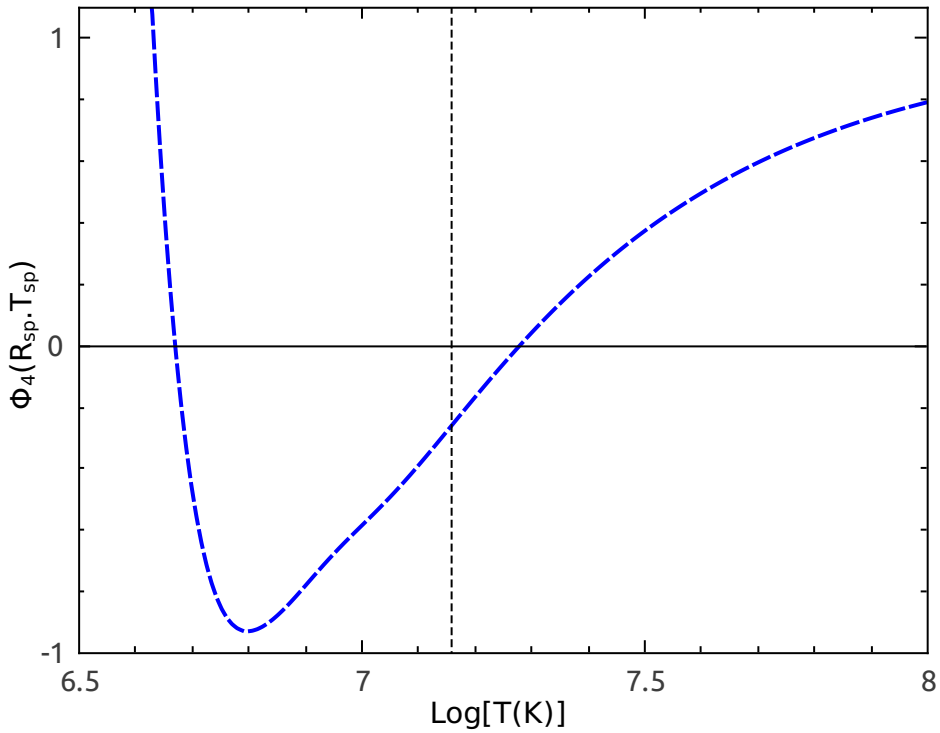

Figure 5.7: Function $\Phi_4(R_{sp}, T_{sp})$ for model H. Thin vertical dashed line marks the value of the adiabatic wind central temperature.

Chapter 6

Concluding Remarks

The aim of this thesis has been to develop a semi-analytic method which allows to study the hydrodynamics of stationary spherically-symmetric winds driven by young super star clusters (SSCs) with an exponential stellar density distribution. Considering a non-homogeneous and more realistic stellar density distribution substantially improves the hydrodynamic model originally proposed by Chevalier & Clegg (1985). This method is described in Chapters 3 and 4. In contrast with previous works, the method allows to calculate the position of the singular point self-consistently.

I verified the semi-analytic code by comparing my results with those obtained in the one-dimensional numeric approach carried out by Ji et al. (2006). Both methods are in excellent agreement in the quasi-adiabatic regime.

The results from the calculations are presented in Chapter 5. The radial profiles for the flow variables: expansion velocity, wind temperature, particle number density, thermal pressure and ram pressure, are presented for a set of input parameters.

Two hydrodynamic regimes are discussed

- The quasi-adiabatic regime, in which the singular point is always located at four times the star cluster core radius. Additionally, the thermal pressure and the ram pressure are equal at three times the star cluster core radius.

- The catastrophic cooling regime, in which strong radiative cooling moves the position of the singular point towards the star cluster center. This is different from the homogeneous case when the singular point is fixed at the star cluster

surface and the stagnation point (R_{st}; the point where the expansion velocity is 0 km s^{-1}), moves from the star cluster center towards the star cluster surface (Tenorio-Tagle et al., 2007).

Radiative cooling leads to the existence of warm (10^4 K) high velocity (of a few hundred to a few thousand km s^{-1}) outflows around young star forming regions. This could be related to the warm isothermal gaseous component found by (Ménard et al., 2009) around star forming galaxies.

I suggest that the catastrophic cooling regime sets in when the solution of equation (4.19) with the larger temperature at the singular point surpasses the adiabatic wind central temperature $T_c^{max} = \frac{(\gamma-1)\mu_{ion}u_{A\infty}^2}{2\gamma k_B}$ and the solution with the smaller temperature must be used.

The semi-analytic method presented in this thesis can be easily extended to other stellar density distributions. In particular, it can be applied to the modified King models suggested by Elson et al. (1987). It would be also instructive to compare the semi-analytic results with 1D and 2D numerical simulations and determine whether the flow outside of the singular point is thermally unstable.

The major results obtained in this thesis are presented in the paper "The Steady State Wind Model for Young Stellar Clusters with an Exponential Stellar Density Distribution" recently accepted for publication in The Astrophysical Journal (astro-ph:1110.0847v1).

Appendices

Appendix A

The Derivative of the Wind Density

From equation (3.8), the wind density is

$$\rho_w = \frac{2q_{mo}R_c^3 A}{u_w r^2} \, . \tag{A.1}$$

where A is a dimensionless term defined as

$$A = \left[1 - \left(1 + \frac{r}{R_c} + \frac{1}{2}\frac{r^2}{R_c^2}\right) e^{-r/R_c}\right] \, . \tag{A.2}$$

The derivative of the wind velocity can be expressed as

$$\frac{d\rho_w}{dr} = \frac{2q_{mo}R_c^3}{u_w r^2}\frac{dA}{dr} + A\frac{d}{dr}\left(\frac{2q_{mo}R_c^3}{u_w r^2}\right), \tag{A.3}$$

where the derivative of the A is

$$\frac{dA}{dr} = \frac{1}{2}\frac{r^2 e^{-r/R_c}}{R_c^3}. \tag{A.4}$$

Thus yields

$$\frac{d\rho_w}{dr} = \frac{q_m}{uw} - \frac{2q_{mo}R_c^3 A}{u_w^2 r^2}\frac{du_w}{dr} - \frac{4q_{mo}AR_c^3}{u_w r^3}. \tag{A.5}$$

Finally, the derivative of the wind density is

$$\frac{d\rho_w}{dr} = \frac{q_m}{u_w} - \frac{\rho_w}{u_w}\frac{du_w}{dr} - \frac{2\rho_w}{r} \tag{A.6}$$

Appendix B

The Derivative of the Local Sound Speed

The local sound speed is defined as

$$c_s^2 = \frac{\gamma P_w}{\rho_w}. \tag{B.1}$$

Applying the chain rule, the derivative of the local sound speed then is

$$\frac{dc_s^2}{dr} = \frac{\gamma}{\rho_s^2}\left(\frac{dP_w}{dr}\rho_w - \frac{d\rho_w}{dr}P_w\right) . \tag{B.2}$$

According to equation 3.10, the derivative of the thermal pressure is

$$\frac{dP_w}{dr} = -\rho_w u_w \frac{du_w}{dr} - q_m u_w. \tag{B.3}$$

Combining B.3 with the derivative of the wind density, derived in equation A.6, finally yields

$$\frac{dc_s^2}{dr} = \frac{du_w}{dr}\left[\frac{c_s^2}{u_w} - \gamma u_w\right] + \frac{q_m}{\rho_w}\left[-\frac{c_s^2}{u_w} - \gamma u_w\right] + \frac{2c_s^2}{r} . \tag{B.4}$$

Appendix C

The Approximate Relations

In this appendix, the approximate relations found for some of the hydrodynamic and star cluster variables in the quasi-adiabatic wind regime are presented.

In Chapter 5, it has been discussed that the ram pressure, P_{RAM}, equals the thermal pressure, P_w, at a radius, $R_{_{RAM}}$, about three times larger than the star cluster core radius R_c. Additionally, it was found that the singular point, R_{sp}, is located at a distance $R_{sp} \approx 4R_c$. The outflow velocity at the singular point is $u_{sp} \approx \frac{1}{2}u_{A\infty}$ (Chevalier & Clegg, 1985), and the wind central temperature is related to the singular point temperature: $T_{sp} \approx \frac{3}{4}T_c$. All these approximate relations are almost insensitive to changes in the input parameters (cf. Table C.1).

Model	R_{sp}/R_c	$R_{_{RAM}}/R_c$	$u_{A\infty}/u_{sp}$	T_c/T_{sp}
A	4.04	3.00	1.99	1.32
B	4.04	3.01	1.99	1.32
C	4.02	3.04	2.14	1.33
D	4.03	3.08	2.05	1.31
E	4.04	3.04	1.99	1.32
F	4.03	3.05	2.07	1.34
G	4.04	3.05	1.99	1.31

Table C.1: Ratios between R_{sp}/R_c, $R_{_{RAM}}/R_c$, $u_{A\infty}/u_{sp}$ and T_c/T_{sp} for models A, B, C, D, E, F and G.

Appendix D

The Isothermal Wind Hydrodynamic Equations

The isothermal wind hydrodynamic equations are derived. Since no temperature gradients are considered, the fluid motion is completely defined by only two differential equations

In the isothermal case, the local sound speed is a constant

$$c_s^2 = \frac{\gamma P_w}{\rho_w}. \tag{D.1}$$

Momentum conservation equation (3.2) is

$$\rho_w u_w \frac{du_w}{dr} = -\frac{dP_w}{dr} - q_m u_w \, , \tag{D.2}$$

Since the local sound speed is a constant, the derivative of the thermal pressure can be calculated analytically from

$$P_w = \frac{\rho_w c_s^2}{\gamma} \tag{D.3}$$

But in order to minimize changes in the numerical code, one can also calculate the thermal pressure from the differential equation

$$\frac{dP_w}{dr} = \frac{P_w}{\rho_w}\frac{d\rho_w}{dr}. \tag{D.4}$$

Using equation (D.4), momentum conservation equation turns into

$$\rho_w u_w \frac{du_w}{dr} = -\frac{P_w}{\rho_w}\frac{d\rho_w}{dr} - q_m u_w \,, \tag{D.5}$$

Combining with equation (A.1), yields

$$\rho_w u_w \frac{du_w}{dr} = -\frac{q_m c s^2}{\gamma u_w} + \frac{2\rho_w c_s^2}{\gamma r} + \frac{\rho_w c_s^2}{\gamma u_w}\frac{du_w}{dr} - q_m u_w \,, \tag{D.6}$$

reordering terms, one can obtain

$$\rho_w u_w \frac{du_w}{dr}\left(u_w - \frac{c_s^2}{\gamma u_w}\right) = -\frac{q_m c_s^2}{\gamma u_w} + \frac{2\rho_w c_s^2}{\gamma r} - q_m u_w, \tag{D.7}$$

and thus yields

$$\frac{du_w}{dr} = \frac{-\frac{q_m c_s^2}{\gamma u_w} + \frac{2\rho_w c_s^2}{\gamma r} - q_m u_w}{\rho_w\left(u_w - \frac{c_s^2}{\gamma u_w}\right)} \,. \tag{D.8}$$

Figure Index

Table Index

References

Arp, H., & Sandage, A. 1985, AJ, 90, 1163

Billett, O. H., Hunter, D. A., & Elmegreen, B. G. 2001, in Bulletin of the American Astronomical Society, Vol. 33, American Astronomical Society Meeting Abstracts, 1329–+

Cantó, J., Raga, A. C., & Rodríguez, L. F. 2000, ApJ, 536, 896

Chevalier, R. A., & Clegg, A. W. 1985, ApJ, 317, 44

Clarke, C. J., & Carswell, R. F. 2007, Principles of Astrophysical Fluid Dynamics (Cambridge University Press)

Elson, R. A. W., Fall, S. M., & Freeman, K. C. 1987, ApJ, 323, 54

Heckman, T. M., Armus, L., & Miley, G. K. 1990, ApJS, 74, 833

Holtzman, J. A., Faber, S. M., Shaya, E. J., Lauer, T. R., Groth, J., Hunter, D. A., Baum, W. A., Ewald, S. P., Hester, J. J., Light, R. M., Lynds, C. R., O'Neil, Jr., E. J., & Westphal, J. A. 1992, AJ, 103, 691

Ji, L., Wang, Q. D., & Kwan, J. 2006, MNRAS, 372, 497

Johnson, H. E., & Axford, W. I. 1971, ApJ, 165, 381

Johnson, K. E., Leitherer, C., Vacca, W. D., & Conti, P. S. 2000, AJ, 120, 1273

King, I. 1962, AJ, 67, 471

Lada, C. J., & Lada, E. A. 2003, ARA&A, 41, 57

Lamers, H. J. G. L. M., & Cassinelli, J. 2007, Introduction to Stellar Winds (Cambridge University Press)

Larsen, S. S., Brodie, J. P., & Hunter, D. A. 2004, AJ, 128, 2295

Leitherer, C., Schaerer, D., Goldader, J. D., González Delgado, R. M., Robert, C., Kune, D. F., de Mello, D. F., Devost, D., & Heckman, T. M. 1999, ApJS, 123, 3

Mayya, Y. D., Romano, R., Rodríguez-Merino, L. H., Luna, A., Carrasco, L., & Rosa-González, D. 2008, ApJ, 679, 404

McCrady, N., Gilbert, A. M., & Graham, J. R. 2003, ApJ, 596, 240

Melnick, J., Moles, M., & Terlevich, R. 1985, A&A, 149, L24

Melo, V. P., Muñoz-Tuñón, C., Maíz-Apellániz, J., & Tenorio-Tagle, G. 2005, ApJ, 619, 270

Ménard, B., Wild, V., Nestor, D., Quider, A., & Zibetti, S. 2009, ArXiv e-prints

Mengel, S., Lehnert, M. D., Thatte, N., & Genzel, R. 2002, A&A, 383, 137

Meurer, G. R., Heckman, T. M., Leitherer, C., Kinney, A., Robert, C., & Garnett, D. R. 1995, AJ, 110, 2665

O'Connell, R. W., Gallagher, III, J. S., & Hunter, D. A. 1994, ApJ, 433, 65

Portegies Zwart, S. F., McMillan, S. L. W., & Gieles, M. 2010, ARA&A, 48, 431

Raga, A. C., Velázquez, P. F., Cantó, J., Masciadri, E., & Rodríguez, L. F. 2001, MNRAS, 559, L33

Raymond, J. C., Cox, D. P., & Smith, B. W. 1976, ApJ, 204, 290

Rockefeller, G., Fryer, C. L., Melia, F., & Wang, Q. D. 2005, ApJ, 623, 171

Rodríguez-González, A., Cantó, J., Esquivel, A., Raga, A. C., & Velázquez, P. F. 2007, MNRAS, 380, 1198

Sarazin, C. L., & White, III, R. E. 1987, ApJ, 320, 32

Silich, S., Tenorio-Tagle, G., & Muñoz-Tuñón, C. 2003, ApJ, 590, 791

Silich, S., Tenorio-Tagle, G., & Muñoz-Tuñón, C. 2007, ApJ, 669, 952

Silich, S., Tenorio-Tagle, G., & Rodríguez-González, A. 2004, ApJ, 610, 227

Tenorio-Tagle, G., Silich, S., Rodríguez-González, A., & Muñoz-Tuñón, C. 2005, ApJ, 620, 217

Tenorio-Tagle, G., Wünsch, R., Silich, S., & Palouš, J. 2007, ApJ, 658, 1196

Weigelt, G., & Baier, G. 1985, A&A, 150, L18

Whitmore, B. C. 2000, ArXiv Astrophysics e-prints

Whitmore, B. C., & Schweizer, F. 1995, AJ, 109, 960

Whitmore, B. C., Zhang, Q., Leitherer, C., Fall, S. M., Schweizer, F., & Miller, B. W. 1999, AJ, 118, 1551

Wünsch, R., Silich, S., Palouš, J., Tenorio-Tagle, G., & Muñoz-Tuñón, C. 2011, ApJ, 740, 75

Wünsch, R., Tenorio-Tagle, G., Palouš, J., & Silich, S. 2008, ApJ, 683, 683